Bistability in a model of mesoderm and anterior mesendoderm specification in

A.M. Middleton, J.R. King, M. Loose

www.elsevier.com/locate/yjtbi

Bistability in a model of mesoderm and anterior mesendoderm specification in *Xenopus laevis*

A.M. Middleton, J.R. King, M. Loose

PII: S0022-5193(09)00238-0
DOI: doi:10.1016/j.jtbi.2009.05.016
Reference: YJTBI 5568

To appear in: *Journal of Theoretical Biology*

Received date: 24 October 2008
Revised date: 10 April 2009
Accepted date: 16 May 2009

Cite this article as: A.M. Middleton, J.R. King and M. Loose, Bistability in a model of mesoderm and anterior mesendoderm specification in *Xenopus laevis*, *Journal of Theoretical Biology*, doi:10.1016/j.jtbi.2009.05.016

Bistability in a model of mesoderm and anterior mesendoderm specification in *Xenopus Laevis*

A. M. Middleton[a,b,*], J.R. King[a], M. Loose[c]

[a] *School of Mathematical Sciences, University of Nottingham, University Park, Nottingham, NG7 2RD, UK*
[b] *CPIB, School of Biosciences, University of Nottingham, Sutton Bonington, LE12 5RD, UK*
[c] *Institute of Genetics, The University of Nottingham, Queen's Medical Centre, Nottingham, NG7 2UH, UK*

Abstract

In this paper we develop a model of mesendoderm specification in *Xenopus Laevis* based on an existing gene regulation network. The mesendoderm is a population of cells that may contribute to either the mesoderm or endoderm. The model that we develop encompasses the time evolution of transcription factor concentrations in a single cell and is shown to have stable steady states that correspond to mesoderm and anterior mesendodermal cell types, but not endoderm (except in cells where *Goosecoid* expression is inhibited). Both *in-vitro* and *in-vivo* versions of the model are developed and analysed, the former indicating how cell fate is determined in large part by the concentration of Activin administered to a cell, with the model results comparing favourably with current quantitative experimental data. A numerical investigation of the *in-vivo* model suggests that cell fate is determined largely by a VegT and β-Catenin pre-pattern, subsequently being reinforced by Nodal. We argue that this sensitivity of the model to a VegT and β-Catenin pre-pattern indicates that a key VegT self-limiting mechanism (for which there is experimental evidence) is absent from the model. Furthermore, we find that the lack of a steady state corresponding to endoderm is entirely consistent with current *in-vivo* data, and that the *in-vivo* model corresponds to mesendoderm specification on the dorsal, but not the ventral, side of the embryo.

1. Introduction

1.1. Background

The development of an embryo from a fertilised egg to a multi-cellular organism proceeds through numerous steps, one of the earliest of which is the establishment of the three primary germ layers, namely mesoderm, endoderm and ectoderm (Alberts et al. (1994); Slack (1991)). Each germ layer contributes to different tissues and organs in the developing animal. Germ layers can be distinguished both morphologically and by the range of genes[1] they express, which may subsequently act to

*Corresponding author
[1] Gene expression corresponds to the synthesis of the protein encoded by a specific gene.

direct the development of the specific tissues. The particular genes expressed within a particular cell are determined in part by the transcription factors (TFs) and signals present: TFs operate in the intracellular domain, and bind directly to a promoter site of a gene (and either activate or repress it), while signals are secreted by cells and regulate genes either in nearby cells or in the originating cell (typically via an intracellular signalling cascade) (Lewin (2007); Alberts et al. (1994)). Thus, a gene encoding a TF or a signal can either repress or activate its target genes, which themselves may encode TFs or signals, leading to a gene regulation network (GRN). Detailed GRNs have been built for a number of single-celled organisms, including *Escherichia Coli* (Shen-Orr et al. (2002); Ma et al. (2004)) and *Saccharomyces Cerevisiae* (Lee et al. (2002)). GRNs are being used increasingly to describe developmental processes in multicellular organisms, including *Caenorhabditis elegans*, Sea Urchin, *Xenopus* and *Drosophila* (Davidson et al. (2002); Loose and Patient (2004); Koide et al. (2005); Platzer and Meinzer (2004)). However, there is a difference in purpose between the GRNs of single-celled and multi-cellular organisms: a GRN within a multi-cellular organism must be able to generate simultaneously a range of cell types in the developing organism. Thus, a multi-cellular organism is likely to possess GRNs dedicated specifically to the task of cell specification. Biological intuition suggests that, in the modelling of cell differentiation, distinct cell types (such as mesoderm or endoderm) can be associated with distinct attractors of a dynamical system (Huang et al. (2005)). Furthermore, a number of mathematical models of GRNs that control cell differentiation have been developed, examples of which include differentiation of haematopoietic stem cells (Roeder and Glauche (2006); Laslo et al. (2006)), including T-cell differentiation (Mariani et al. (2004); Yates et al. (2004)), and segment specification in *Drosophila* (von Dassow et al. (1998)).

1.2. Preliminaries

The *Xenopus laevis* mesendoderm network described in Loose and Patient (2004) (and subsequently in Koide et al. (2005)) involves approximately 50 transcription factors (TFs) and signalling-molecule species. Mesoderm largely corresponds to *Brachyury* expressing cells and endoderm to those expressing *Mix.1* (Lemaire et al. (1998)). The dorsal mesoderm, which gives rise to anterior (head forming) structures, is associated with cells expressing *Goosecoid* (Cho et al. (1991)) (the majority of these cells also express *Brachyury*, although this overlap in expression is almost completely lost in stage 12[2] embryos (Artinger et al. (1997))) . Thus, ventral mesendoderm is associated with cells expressing both *Mix.1* and *Brachyury*, whereas dorsal mesendoderm with cells expressing *Mix.1*, *Brachyury* and *Goosecoid*. At present, it is not clear whether cells co-expressing *Goosecoid* and *Mix* (anterior mesendoderm) segregrate (see Section 5 for further details), although such a separation

[2]Stage 12 corresponds with the completion of gastrulation.

Figure 1: Cartoon of experimental observations. (*i*) (Left) At stage 10 (9 hours after fertilisation) the expression domain of *Mix.1/Goosecoid* (anterior mesendoderm) overlaps that of *Brachyury* (endoderm), with this overlap representing the mesendoderm (Latinkic and Smith (1999); Wardle and Smith (2004); Lemaire et al. (1998)). (Middle) By stage 10.5 (11 hours after fertilisation) the mesendoderm has differentiated so that the *Brachyury* expressing cells form a separate population to the *Mix/Goosecoid* co-expressing ones (Wardle and Smith (2004); Lemaire et al. (1998)). (Right) Experimental results (Sander et al. (2007)) show *Goosecoid* expression extends to the ventral region in embryos lacking *Vent-1/2*. The large arrow indicates the area of the embryo for which the *in vivo* model is relevant; see text for details. (*ii*) Spatial distribution of maternal factor β-Catenin (Schohl and Fagotto (2002)) and VegT (see Section 1.2 for references).

would correspond to the formation of anterior mesoderm and endoderm. We will refer to cells co-expressing *Mix.1* and *Goosecoid* as anterior (*i.e.* head forming) mesendoderm. On the ventral side of the embryo, the mesendoderm can contribute either to the mesoderm or the endoderm (Lemaire et al. (1998)). On the dorsal side, it separates into mesoderm and anterior mesendoderm (Lemaire et al. (1998); Latinkic and Smith (1999)). **The expression domains of *Mix.1*, *Brachyury* and *Goosecoid* are illustrated in Figure 1(*i*)**. Given these data, the underlying network should have the ability to differentiate into either mesoderm, endoderm or anterior mesendoderm. The method used in Loose and Patient (2004) to construct the mesendoderm GRN relies on a comprehensive collation of all the data known to be associated with dorsal mesendoderm specification in *Xenopus laevis* (so it is possible that pertinent interactions and genes are missing). In particular, the network does not contain genes associated with ventral patterning (most notably BMP-4 and its targets, including Vent-1 and Vent-2 (Sander et al. (2007)), which will be important in what follows).

The mesendoderm GRN in Loose and Patient (2004) is complex, involving a considerable number of interactions. The most important genes within this network (in the current context) are *Brachyury*, *Mix.1*, *Goosecoid*, the *Nodal* family, while key maternal factors are VegT and β-Catenin. *Mix.1* is a member of the *Mix* homeobox family, which consists of seven *Mix*-type genes (*Mixer, Mix.1-2, Bix.1-4*), each of which encodes a transcription factor (Loose and Patient (2004)). A prominent interaction within the network is the mutual repression between *Mix.1* and *Brachyury* (Lemaire et al. (1998), Latinkic and Smith (1999)), this being the only source of competition between mesoderm and endoderm in the full network (Loose and Patient (2004)). Experimental evidence (Lemaire et al. (1998)) suggests that it is this competition between the two germ layers which drives the differentiation of a mesendoderm cell into either mesoderm, endoderm or anterior mesendoderm. We note that there is evidence that the repression of *Brachyury* by Mix.1 may be indirect (Latinkic and Smith (1999)), whereby Mix.1 activates *Goosecoid*; Goosecoid in turn represses *Brachyury* directly (see Loose and Patient (2004); Latinkic and Smith (1999) and references therein). On the other hand, it is not known whether the repression of *Mix.1* by Brachyury is direct or indirect, and for simplicity we shall assume it to be the former (see Figure 3 in Loose and Patient (2004)). We also

note that Goosecoid represses its own gene (Loose and Patient (2004)). Another key gene family in the mesendoderm GRN is *Nodal*, comprising six members (*Xnr1-6*) (Loose and Patient (2004)) each of which encodes an Activin-like signal (see Green (2002) for a review). The differentiation of mesendodermal cells depends on the concentration of Activin-like signalling: at low concentrations of Activin a cell expresses *Brachyury* (*i.e.* is mesoderm). As the concentration of Activin increases, the *Brachyury* concentration increases to a maximum, beyond which it declines to negligible levels. A cell expresses *Goosecoid* and *Mix.1* (*i.e.* is anterior mesendoderm) at higher concentrations of Activin. This response to Activin has been observed in both single-cell (Gurdon et al. (1999); Papin and Smith (2000)) and whole-tissue (Gurdon et al. (1994, 1995, 1996); Green et al. (1994)) experiments. The maternal factors **VegT and β-Catenin are both important for the initiation of the mesendoderm network (Xanthos et al. (2001); Heasman (2006); Schohl and Fagotto (2003)). Early VegT depletion experiments performed by Zhang et al. (1998) showed that embryos with a reduced concentration of VegT fail to form anterior mesendoderm, with the mesoderm marker *Brachyury* shifting its expression from the equatorial to the vegetal region (*i.e.* to include the region that would usually form endoderm and anterior mesendoderm). Moreover, further experiments with a more effective VegT depletion technique resulted in the abolition of both mesoderm and anterior mesendoderm (Kofron et al. (1999)), suggesting that VegT is necessary for both Mix and Brachyury expression. Thus, on the assumption that the technique used in the experimental series of Zhang et al. (1998) reduced the level of VegT in a manner that is not too non-uniform, these observations are consistent with the hypothesis that there exists a gradient of VegT, with its concentration decreasing between the presumptive mesoderm and anterior mesendoderm. β-Catenin signalling is largely restricted to the presumptive mesoderm (Schohl and Fagotto (2002)). The spatial distribution of VegT and β-Catenin is illustrated in Figure 1(*ii*).**

In this paper we propose a mathematical model for a simplified *Xenopus laevis* mesendoderm GRN that is based on the full gene regulation network from Loose and Patient (2004). We observe that the complexity of the full network in Loose and Patient (2004) is largely a consequence of the *Mix* and *Nodal* gene families. To simplify our analysis, we shall therefore treat each of these gene families as a single gene. This reduction is supported by the observation that in both mouse and humans only one *Nodal* and one *Mix* family member have been identified (Guo et al. (2002); Hart et al. (2002); Mohn et al. (2003); Zhou et al. (1993)). Thus, in our model the six *Nodal* family members are replaced by a single *Nodal* gene. Similarly, the seven *Mix*-type genes are treated as a single *Mix* gene. The underlying topology of the full *Xenopus* mesendoderm network is then

Figure 2: The simplified *in-vivo* network: the gene families *Mix* and *Nodal* are each treated as a single node in the network (see main text). The network is organised into two components, the maternal (green box) and the zygotic (yellow boxes). Arrow and bar heads represent, respectively, activation and repression. The 'A' indicates that an input is, in Boolean terms, an 'AND' gate. Otherwise, multiple inputs consisting of only one type (repression or activation) correspond to an 'OR' gate. When both types are present, the repression and activation inputs are treated as two 'OR' gates coupled by an 'AND' gate (see text). 'S' indicates a gene that encodes a signal (otherwise it encodes a TF). VegT and β-Catenin activate *Nodal*, and together with Nodal activate the remaining downstream genes. β-Catenin and Nodal respectively activate *Siamois* and *Lim1* (light yellow box). The red and blue boxes highlight the fact that *Mix* (together with *Goosecoid*) and *Brachyury* (together with *eFGF*) form two competing gene subgroups through mutual repression.

Figure 3: The simplified (*in vitro*) network: the Nodal signal is simulated by bathing either whole or dissociated animal caps in Activin. Animal cap cells lack the maternal factors VegT and β-Catenin. Note that the downstream network (consisting of *Brachyury*, *Goosecoid* and *Mix*) is as in Figure 2.

described by combining the inputs and outputs of each of these gene family members in the network of Loose and Patient (2004), this leading to our simplified network shown in Figure 2. Here we model both *in-vivo* (where maternal factors and Nodal regulate the expression of the downstream targets) and *in-vitro* (where Activin is used to simulate Nodal signalling, as in the dose response experiments described above) cases; the latter network is shown in Figure 3.

In summary, our network contains the key features of the full *Xenopus* GRN, notably the mutual repression of *Mix* and *Brachyury* (via *Goosecoid*) and the autoregulation of *Nodal*. We analyse this model below, showing that it can produce dynamics that are representative of the full mesendoderm GRN; it is worth emphasising that the required properties for the dorsal side of the embryo (*i.e.* mesendoderm contributes to mesoderm and anterior mesendoderm) arise directly from this natural choice of simplified network: our first pass at formulating the network required no *post hoc* fine tuning. **The model is shown to have stable steady states that correspond to mesoderm and anterior mesendodermal cell types, but not endoderm (except in cells where *Goosecoid* expression is inhibited). Both *in-vitro* and *in-vivo* versions of the model are developed and analysed. Our findings suggest that the simplified GRN (Figures 2-3) embodies a core mechanism that allows a cell to determine its position in a gradient of either Activin (in the *in-vitro* case) or VegT (in the *in-vivo* case). Thus, in the context of**

Table 1: A summary of gene products present in the full *Xenopus* mesendoderm GRN (see text and Loose and Patient (2004)), their type (transcription factor or signal) and family name. The final column provides the notation in the model for the associated protein concentrations. Activin does not appear in either the full or the simplified *in-vivo* networks (see Figure 2), but is used to simulate Nodal expression *in vitro* and is incorporated in the model of Section 3 (see Figure 3).

classical developmental biology, this paper is concerned with how a morphogen[3] gradient may be interpreted by a line of cells, rather than how the gradient is formed. The latter problem has received a considerable attention over the last few decades, for example see Kerszberg and Wolpert (1998). A general discussion on the patterning of the three primary germ layers is provided in Meinhardt (2001), together with hypothetical models of the activator-inhibitor reaction-diffusion type, with (in the case of mesoderm formation) *eFGF* (which is in a positive feedback loop with *Brachyury*) being postulated as a possible 'activator', but the inhibitor not having been identified.

Finally, the network used in Loose and Patient (2004) clearly cannot be expected to account for mesendoderm differentiation on the ventral side of the embryo (where mesendoderm contributes to mesoderm and endoderm) and we propose that this is due in large part to the absence of a key interaction from our model, namely the mutually antagonistic loop between *Goosecoid* and the ventrally expressed *Vent-1/2* (Sander et al. (2007); Saka, Y. and Smith, J.C. (2007)).

2. Model formulation

2.1. The Model

In this Section we write down an appropriate set of governing equations for our specific (simplified) GRN. **Our model of the *in-vivo* case represents a single cell embedded in a population of identical cells, allowing us to include signal-mediated autoregulation in the model (the relevant ones being Nodal and eFGF) and to neglect spatial effects (*i.e.* effects from signal diffusion will be negligible if all cells within a population are identical)**. In contrast, the *in-vitro* case cells are dissociated and bathed in Activin, as in the experiments of Papin and Smith (2000); Gurdon et al. (1999). Here, **any** signals secreted by a cell are assumed to be too dilute to regulate their downstream targets, and so we neglect *eFGF* and *Nodal* expression (contrast Figures 2 and 3). **We formulate ODEs for each of protein species and base the underlying logic of our simplified network (see Figure 2) upon various experimental observations, some of which are outlined above; further details are given in Middleton, A. (2007) and in the interests of brevity we forego a detailed discussion of the issue.**

2.1.1. In-vitro model

The *in-vitro* model comprises the time evolution of Brachyury (B), Mix (M) and Goosecoid (G) TF concentrations in a single (dissociated) cell. It has been shown (Dyson and Gurdon (1998)) that only a small proportion of the relevant receptors is required to be Activin bound for *Goosecoid* and

[3] A morphogen is a signal that can form a gradient through out a field of cells and determine the arrangement and fate of responding cells according to its concentration.

Brachyury expression to be induced. Furthermore, it was shown in Bourillot et al. (2002) that this initial level of Activin treatment is 'remembered' by the phosphorylation of one of its intracellular mediators, Smad2 (a transcription factor), *i.e.* phosphorylated Smad2 is maintained at a constant concentration. It is likely that this is a consequence of the Activin-receptor complex remaining active for a long period of time (Bourillot et al. (2002)). Furthermore, the level of phosphorylated Smad2 has been observed to be proportional to the concentration of Activin administered (Shimizu and Gurdon (1999); Dyson and Gurdon (1998); Bourillot et al. (2002)). Therefore, we take the concentration of Activin (A) to be a prescribed constant in the intracellular model, being a proxy for the relevant intracellular mediators. The relevant gene interactions are illustrated in Figure 3. From this point on, our notation will be as follows: a gene $\mathbf{X}$ has protein product $\bar{\mathbf{X}}$ (a signal or TF), with concentration X. The positive constants $\lambda_{Y,X}$ and μ_X are respectively the maximum rate of production of $\bar{\mathbf{X}}$ induced by $\bar{\mathbf{Y}}$ and the rate of its turnover. The governing equations are taken to be

$$\dot{B} = \lambda_{A,B}\mathcal{H}\left(\frac{A}{\theta_{A,B}}\right)\left\{1-\mathcal{H}\left(\frac{G}{\theta_{G,B}}+\frac{M}{\theta_{M,B}}\right)\right\}-\mu_B B, \tag{1a}$$

$$\dot{G} = \lambda_{M,G}\mathcal{H}\left(\frac{M}{\theta_{M,G}}\right)\left\{1-\mathcal{H}\left(\frac{G}{\theta_{G,G}}\right)\right\}-\mu_G G, \tag{1b}$$

$$\dot{M} = \lambda_{A,M}\mathcal{H}\left(\frac{A}{\theta_{A,M}}\right)\left\{1-\mathcal{H}\left(\frac{B}{\theta_{B,M}}\right)\right\}-\mu_M M, \tag{1c}$$

where $\mathcal{H}$ is the Hill function

$$\mathcal{H}(x) = \frac{x^m}{x^m+1}, \tag{2}$$

with Hill coefficient $m \geq 1$ (this being a measure of the cooperativity of TF-DNA binding, see Alon (2007); Middleton, A. (2007) for further details). We note that in the limit $m \to \infty$ we have $\mathcal{H}(x) \to H(x)$, the step function defined by $H(x) = 0$ for $0 \leq x < 1$, $H(x) = 1/2$, for $x = 1$ and $H(x) = 1$ for $x > 1$ (we emphasise that this is a translated version of the usual Heaviside step function). Thus, $\theta_{X,Y}$ is the concentration threshold at which $\bar{\mathbf{Y}}$ can transcriptionally regulate $\mathbf{X}$ in the large m limit. Initial conditions

$$M(0) = B(0) = G(0) = 0, \tag{3}$$

are chosen to represent the initial state of an animal cap cell, where none of these factors are expressed in the absence of exogenous Activin.

2.1.2. In-vivo model

The *in-vivo* model encompasses the time evolution of VegT (V), β-Catenin (C) (these being maternal factors), Mix (M), Brachyury (B), Nodal (N), Goosecoid (G), Lim.1 (L), and Siamois

(S) concentrations in a single cell. The maternal factors are treated as intracellular deposits of protein with a prescribed turnover rate. *Nodal* family members *Xnr1,2,4,5,6* (*Xnr3* is expressed in ectoderm and appears to have a separate developmental role) are initially regulated by the maternal factors VegT and β-Catenin (Rex et al. (2002); Xanthos et al. (2001)). Xnr1, 2 and 4 can activate their own genes (see Loose and Patient (2004); Rex et al. (2002)) and this can be enhanced by β-Catenin. The model for the regulation of our single *Nodal* gene is motivated by these properties: *Nodal* can be activated by either VegT (leading to the $\lambda_{V,N}$ term in (4c)) or by Nodal signalling (the $\lambda_{N,N}$ term), the latter being enhanced by β-Catenin (the $\lambda_{C,N}$ term). The equations governing the concentrations of VegT (V), β-Catenin (C) and Nodal (N) are as follows, a summary of the notation used being given in Table 1:

$$\dot{C} = -\mu_C C, \tag{4a}$$

$$\dot{V} = -\mu_V V, \tag{4b}$$

$$\dot{N} = \lambda_{V,N}\mathcal{H}\left(\frac{V}{\theta_{V,N}}\right) + \lambda_{N,N}\left(1 + \lambda_{C,N}\mathcal{H}\left(\frac{C}{\theta_{C,N}}\right)\right)\mathcal{H}\left(\frac{N}{\theta_{N,N}}\right) - \mu_N N, \tag{4c}$$

while the concentrations of Siamois (S) and Lim1 (L) are governed by

$$\dot{S} = \lambda_{C,S}\mathcal{H}\left(\frac{C}{\theta_{C,S}}\right) - \mu_S S, \tag{5a}$$

$$\dot{L} = \lambda_{N,L}\mathcal{H}\left(\frac{N}{\theta_{N,L}}\right) - \mu_L L. \tag{5b}$$

Given the solution to these subsystems we can then solve the following equations for the system comprising eFGF (E), Brachyury (B), Goosecoid (G), and Mix (M):

$$\dot{E} = \lambda_{B,E}\mathcal{H}\left(\frac{B}{\theta_{B,E}}\right) - \mu_E E, \tag{6a}$$

$$\dot{B} = \left\{\lambda_{E,B}\mathcal{H}\left(\frac{E}{\theta_{E,B}}\right) + \lambda_{V,B}\mathcal{H}\left(\frac{V}{\theta_{V,B}}\right) + \lambda_{N,B}\mathcal{H}\left(\frac{N}{\theta_{N,B}}\right)\right\} \left\{1 - \mathcal{H}\left(\frac{G}{\theta_{G,B}} + \frac{M}{\theta_{M,B}}\right)\right\} - \mu_B B, \tag{6b}$$

$$\dot{G} = \left\{\lambda_{LI,B}\mathcal{H}\left(\frac{L}{\theta_{L,G}}\right)\mathcal{H}\left(\frac{I}{\theta_{I,G}}\right) + \lambda_{M,G}\mathcal{H}\left(\frac{M}{\theta_{M,G}}\right)\right\} \left\{1 - \mathcal{H}\left(\frac{G}{\theta_{G,G}}\right)\right\} - \mu_G G, \tag{6c}$$

$$\dot{M} = \left\{\lambda_{V,M}\mathcal{H}\left(\frac{V}{\theta_{V,M}}\right) + \lambda_{N,M}\mathcal{H}\left(\frac{N}{\theta_{N,M}}\right)\right\}\left\{1 - \mathcal{H}\left(\frac{B}{\theta_{B,M}}\right)\right\} - \mu_M M. \tag{6d}$$

In our *in-vivo* model, the only factors initially present are VegT and β-Catenin. As indicated in Section 1, different regions of the embryo are distinguished in the simulations by choosing different initial conditions for VegT and β-Catenin (*i.e.* different values of V_0 and C_0 in (7)). The chosen

initial conditions are

$$\begin{aligned} &C(0)=C_0, \quad V(0)=V_0, \quad N(0)=0, \quad S(0)=0, \\ &L(0)=0, \qquad E(0)=0, \qquad B(0)=0, \quad G(0)=0, \quad M(0)=0, \end{aligned} \tag{7}$$

where $C_0, V_0 \geq 0$ denote the initial levels of β-Catenin and VegT in the region of the embryo under consideration.

2.2. Nondimensionalisation

We nondimensionalise time according to $\tau = \mu_B t$, *i.e.* with the timescale of Brachyury (B) turnover. Purely for notational simplicity, we relabel the following threshold parameters:

$$\begin{aligned} &\theta_X \equiv \theta_{X,B}, \quad \theta_G \equiv \theta_{G,B}, \quad \theta_B \equiv \theta_{B,E}, \quad \theta_E \equiv \theta_{E,B}, \quad \theta_L \equiv \theta_{L,G}, \\ &\theta_I \equiv \theta_{S,G}, \quad \theta_M \equiv \theta_{M,B}, \quad \theta_V \equiv \theta_{V,N}, \quad \theta_C \equiv \theta_{C,N}, \quad \theta_S \equiv \theta_{S,N}, \end{aligned} \tag{8}$$

where $X = A$ (*in-vitro* case) or $X = N$ (*in-vivo* case). Then, for each gene $\mathbf{Z}$ in the simplified network, the dimensionless concentration of $\bar{\mathbf{Z}}$ is based on the threshold level θ_Z given in (8), being defined by $\hat{Z} \equiv Z/\theta_Z$. The remaining dimensionless thresholds are $\hat{\theta}_{Z,X} \equiv \theta_{Z,X}/\theta_Z$. The dimensionless rates of production and turnover are defined respectively by $\hat{\lambda}_{Y,Z} \equiv \lambda_{Y,Z}/\theta_Z\mu_B$ and $\hat{\mu}_Z \equiv \mu_Z/\mu_B$. For each protein we have several (dimensionless) parameters in the model, associated with thresholds ($\hat{\theta}$) and rates of production ($\hat{\lambda}$) and decay ($\hat{\mu}$). While we do not have experimental values for these, we wish to understand the qualitative dynamics of the model and to identify which parameters play the most significant roles. 'Default' parameter values used (*i.e.* those used in the simulations unless otherwise stated) are summarised in Table 2. Parameters were chosen so that (10)-(12) is bistable, with stable steady states corresponding to mesoderm and anterior mesendoderm. Furthermore, the thresholds $\theta_{X,M}$ and $\theta_{V,M}$ were chosen to be greater than unity so that whether the system (subject to initial conditions (3) or (7)) evolves to the mesoderm or to the anterior mesendoderm steady state depends on the concentration of Activin ($X = A > 0$) or of VegT ($V_0 > 0$), in the *in-vitro* or *in-vivo* cases respectively; see Sections 3.2 and 4.2. Unless otherwise stated, steady state solutions were computed with the computer package `Xppaut` (Ermentrout (2002)) which uses pseudoarclength continuation to determine bifurcation curves and time dependent ones with `Matlab` routine `ode15s` for stiff problems.

2.2.1. In-vitro model

The dimensionless *in-vitro* model (1), upon dropping hats, takes the form

$$\dot{B} = \lambda_{A,B}\mathcal{H}(A)\{1-\mathcal{H}(G+M)\} - B, \tag{9a}$$

$$\dot{G} = \lambda_{M,G}\mathcal{H}\left(\frac{M}{\theta_{M,G}}\right)\left\{1-\mathcal{H}\left(\frac{G}{\theta_{G,G}}\right)\right\} - \mu_G G, \tag{9b}$$

$$\dot{M} = \lambda_{A,M}\mathcal{H}\left(\frac{A}{\theta_{X,M}}\right)\left\{1-\mathcal{H}\left(\frac{B}{\theta_{B,M}}\right)\right\} - \mu_M M. \tag{9c}$$

2.2.2. In-vivo model

Upon dropping hats, equations (4)-(6) take the dimensionless form

$$\dot{C} = -\mu_C C, \qquad \dot{V} = -\mu_V V, \tag{10a}$$

$$\dot{N} = \left\{\lambda_{V,N}\mathcal{H}\left(\frac{V}{\theta_{V,N}}\right) + \lambda_{N,N}\mathcal{H}\left(\frac{N}{\theta_{N,N}}\right)\left(1+\lambda_{C,N}\mathcal{H}\left(\frac{C}{\theta_{C,N}}\right)\right)\right\} - \mu_N N, \tag{10b}$$

Table 2: A summary of the dimensionless parameters and their chosen (default) values. $X = A$ (*in-vitro*) or N (*in-vivo*).

and

$$\dot{S} = \lambda_{C,S}\mathcal{H}\left(\frac{C}{\theta_{C,S}}\right) - \mu_S S, \qquad \dot{L} = \lambda_{N,L}\mathcal{H}\left(\frac{N}{\theta_{N,L}}\right) - \mu_L L, \tag{11}$$

together with the fourth-order downstream system:

$$\dot{E} = \lambda_{B,E}\mathcal{H}(B) - \mu_E E, \tag{12a}$$

$$\dot{B} = \left\{\lambda_{E,B}\mathcal{H}(E) + \lambda_{V,B}\mathcal{H}\left(\frac{V}{\theta_{V,B}}\right) + \lambda_{X,B}\mathcal{H}(X)\right\}\{1 - \mathcal{H}(G+M)\} - B, \tag{12b}$$

$$\dot{G} = \left\{\lambda_{LS,B}\mathcal{H}(L)\,\mathcal{H}(S) + \lambda_{M,G}\mathcal{H}\left(\frac{M}{\theta_{M,G}}\right)\right\}\left\{1 - \mathcal{H}\left(\frac{G}{\theta_{G,G}}\right)\right\} - \mu_G G, \tag{12c}$$

$$\dot{M} = \left\{\lambda_{V,M}\mathcal{H}\left(\frac{V}{\theta_{V,M}}\right) + \lambda_{X,M}\mathcal{H}\left(\frac{X}{\theta_{X,M}}\right)\right\}\left\{1 - \mathcal{H}\left(\frac{B}{\theta_{B,M}}\right)\right\} - \mu_M M, \tag{12d}$$

where the dots now represent differentiation with respect to τ. The subsystems (10)-(12) can be solved sequentially with (10) implying that the concentration of Nodal is governed by the single non-autonomous differential equation

$$\dot{N} = \left\{\lambda_{V,N}\mathcal{H}\left(\frac{V_0 \mathrm{e}^{-\mu_V \tau}}{\theta_{V,N}}\right) + \lambda_{N,N}\mathcal{H}\left(\frac{N}{\theta_{N,N}}\right)\left(1 + \lambda_{C,N}\mathcal{H}\left(\frac{C_0 \mathrm{e}^{-\mu_C \tau}}{\theta_{C,N}}\right)\right)\right\} - \mu_N N. \tag{13}$$

3. The *in-vitro* model

3.1. Steady-state analysis

3.1.1. Preliminaries

This Section is concerned primarily with the steady states of the *in-vitro* model (system (9)). As we shall see, the model can imply that a sharp switch between the two cell types occurs as the concentration of Activin (A) is increased. However, for $m = 1$, (9) is monostable, with the steady states of B, M and G increasing monotonically with A; the stable steady state corresponds to 'mesendoderm' (whereby both *Mix* and *Brachyury* are expressed in significant amounts). Thus, for $m = 1$, competition between Brachyury and Mix is not sufficiently effective to create exclusivity. It has been shown in other contexts that simple genetic regulatory circuits consisting of two mutually inhibiting factors (Gardner et al. (2000); Cinquin and Demongeot (2002)) can be bistable provided the binding cooperativity of the various factors is greater than unity (as can those comprising a single positive feedback loop (Becskei et al. (2001))). These observations motivate us to proceed with the case $m > 1$, it being noteworthy that such co-operativity is required if the model is to reproduce the known function of the network.

3.1.2. Steady-state solutions for fixed Activin (A) concentration

Given the large number of parameters in the model, a complete survey of parameter space has not been performed. Intuitively, however, we can reason as follows: the genes *Mix* (**M**) (together with *Goosecoid*) and *Brachyury* (**B**) are in competition, and so the parameters $\lambda_{A,M}$, $\lambda_{A,B}$ (which dictate the rates of production of their respective protein products in response to Activin) must be chosen such that both fates (mesoderm and anterior mesendoderm) are available to a cell. Plotted

Figure 4: Numerical investigation of the effects of mutual inhibition of *Mix* and *Brachyury*, as described by (9), for $A = 5$. (i) As $\lambda_{A,B}$ is increased the system passes through two fold bifurcations: these mark in turn the appearance of a stable steady state branch corresponding to mesoderm (thick solid line) and the extinction of that corresponding to anterior mesendoderm (thin solid line) through coalescence with the unstable steady state (dashed line). The unstable branch could be interpreted as mesendoderm, although this state would never as it stands be realised in practice. Parameter regimes near a fold may be biologically undesirable as these will be strongly sensitive to noise. (ii) Bifurcation structure of (9) plotted in the $(\lambda_{A,B}, \lambda_{A,M})$ plane for $\theta_{G,G} = 10^2$ (black line), $\theta_{G,G} = 1$ (grey line) and $\theta_{G,G} = 0.1$ (light grey line). Parameters are as in Table 2, unless stated otherwise.

in Figure 4 (i)-(iii) are steady-state solutions of (9) for a range of $\lambda_{A,B}$. The system is bistable, the upper and lower branches being associated with mesoderm and anterior mesendoderm respectively. **We recall that Goosecoid can down regulate its own gene (see Figure 2). As illustrated in Figure 4(ii), the strength of the *Goosecoid* negative loop (represented by $\theta_{G,G}$, with $\theta_{G,G} \gg 1$ corresponding to weak feedback) can tune the size of the bistable regime.** These results indicate that the system (12) can have distinct stable steady states that correspond to mesoderm and anterior mesendoderm. By exploring the basins of attraction of each, we can thus investigate how a cell might determine its fate.

3.2. Time-dependent solutions to the in-vitro model

To compare our *in-vitro* model quantitively with (single-cell) experimental results from Gurdon et al. (1999) and Papin and Smith (2000), we now explore the effects of increasing the dose A of Activin being administered to a cell, numerical results for (9) being shown in Figure 5. Recall that initial conditions are chosen such that $M(0) = B(0) = G(0) = 0$ (this choice being representative of the initial state of an animal cap cell). For low A solutions evolve to the mesoderm branch. As A is increased it passes through a critical value A^{c} (say), whereby for $A > A^{\mathrm{c}}$ solutions evolve to the anterior mesendoderm branch. For $A < A^{\mathrm{c}}$, M and G grow slowly and so cannot compete with B (Figure 5(i)). For values of A close to A^{c}, solutions exhibit a mesendoderm phase (where both Mix and Brachyury are expressed at non-negligible levels), prior to the cell settling on a particular fate (Figure 5(ii)); for the non-generic case $A = A^{\mathrm{c}}$ the solution evolves to the unstable steady state. For $A > A^{\mathrm{c}}$, B initially grows faster than M and G, but the subsequent increased growth rates of M and G allow them, in combination, to compete with B, causing its subsequent downregulation (Figure 5(iii)). In the model the mesendoderm phase is much longer in duration if A close to A^{c} than in other parameter regimes. We discuss this observation further in Section 5.

For given initial data, the value of A thus determines whether solutions to (9) evolve to the steady state branch representing mesoderm or anterior mesendoderm. Representative simulations are shown in Figure 6. Such solutions are in good qualitative agreement with the data found in Gurdon et al. (1999) and Papin and Smith (2000). **In these experiments, disaggregated cells are treated with various concentrations of Activin. Initially, both *Brachyury* and *Goosecoid* expression levels increase monotonically with the concentration of Activin (compare Figure 1A in Papin and Smith (2000) to Figure 6(i) here). At later times, however, the expression profiles of the two genes are refined: at low concentrations of Activin, *Brachyury* expression levels increase to a maximum, beyond which they declines to negligible levels. A cell expresses *Goosecoid* and *Mix.1* (is anterior mesendoderm) at high concentrations of Activin (compare Figure 1C in Papin and Smith (2000) to Figure 6(ii) here). We note that a virtually identical response can be observed in Activin treated cell-aggregates (Papin and Smith (2000))**.

Figure 5: Time evolution of (9) for various A, showing B (solid line), G (dot-dash line) and M (dashed line). (*i*) A low value of A causes the system to evolve to the mesoderm steady state branch. (*ii*) A larger A (just above the critical value A^{c}) leads to the system exhibiting a mesendoderm time scale (with solutions close to the unstable steady state), but with the system ultimately evolving to the anterior mesendoderm steady state. (*iii*) A further increase in A causes B to drop rapidly to a negligible concentration (again corresponding to anterior mesendoderm). Other parameters were chosen as in Table 2.

Figure 6: Numerically-computed solutions to (9) as functions of A for various τ. (*i*) Initially, M (dashed line), G (dot-dash line) and B (solid line) are expressed for all A. (*ii*)-(*iii*) As time increases, concentration profiles are refined as solutions tend to mesoderm and anterior mesendoderm steady states for low and high concentrations of A, respectively. We note that (*iii*) does not exhibit a true discontinuity, though one is approached as $\tau \to \infty$. Other parameters were chosen as in Table 2.

3.3. Understanding differentiation: a reduced system

3.3.1. Preliminaries

We now seek to provide further insight into the long-term behaviour of system (9). We rescale the rates of production and turnover of Goosecoid such that

$$\lambda_{M,G} \mapsto \frac{\lambda_{M,G}}{\epsilon} \qquad\qquad \mu_G \mapsto \frac{\mu_G}{\epsilon} \tag{14}$$

where $0 < \epsilon \ll 1$. Representative numerical solutions are given in Figure 7. Decreasing ϵ from one to 10^{-9} causes the basins of attraction of mesoderm and anterior mesendoderm steady states to shift such that solutions evolve to the anterior mesendoderm branch for a slightly lower value of A. Nevertheless, the qualitative behaviour of the two cases is very similar.

3.3.2. A reduced model of mesendoderm differentiation

We now explore the leading-order behaviour of (9) using the rescaling (14) with $\tau = O(1)$, whereby as $\epsilon \to 0$ we have

$$\dot{B} = \left\{\lambda_{E,B}\mathcal{H}\left(E\right) + \lambda_{A,B}\mathcal{H}\left(A\right)\right\}\left\{1 - \mathcal{H}\left(G + M\right)\right\} - B, \tag{15a}$$

$$\dot{M} = \lambda_{N,M}\mathcal{H}\left(\frac{A}{\theta_{A,M}}\right)\left\{1 - \mathcal{H}\left(\frac{B}{\theta_{B,M}}\right)\right\} - \mu_M M, \tag{15b}$$

with $G \equiv G(M)$ set to its quasi-steady state

$$G(M) = \frac{\lambda_{M,G}}{\mu_G}\mathcal{H}\left(\frac{M}{\theta_{M,G}}\right)\left\{1 - \mathcal{H}\left(\frac{G}{\theta_{G,G}}\right)\right\}. \tag{16}$$

We note that there is a unique solution G to (16) for each M (see Figure 8 for a representative solution curve).

The virtue of the current limit is that the model reduces to a second-order system, (15). Representative phase planes are given in Figure 9, these being numerical solutions to (15)-(16). For the parameter choices made, there are two stable steady states, one representing mesoderm and the other anterior mesendoderm. The stable manifold of the saddle point provides the separatrix between the two basins of attraction. We note that $A = A^{\mathrm{c}}$ is the concentration of Activin for which the separatrix crosses the origin, so that trajectories passing through the origin tend to the mesoderm and

Figure 7: Dose response curves of (9) for fast Goosecoid production ($\lambda_{M,G}/\epsilon$) and turnover (μ_G/ϵ) with $\epsilon = 1$ (solid lines), $\epsilon = 10^{-9}$ (dashed lines). Other parameters (including $\lambda_{M,G}$ and μ_G, even through they have a different meaning here – see (14)) were chosen as in Table 2.

Figure 8: For each M there is a unique root $G \equiv G(M)$ to (16). Parameter values were chosen as in Table 2.

Figure 9: Phase plane plots of (15) for various A. (*i*)-(*iii*) Nullclines (dot-dashed lines) intersect at the three equilibrium points. The stable manifold (grey dashed line) of the saddle point acts as the separatrix between the two basins of attraction. The trajectories (bold lines) leaving $(0,0)$ evolves to the mesoderm steady state for $A = 1.7$. For $A = 3$ the separatrix is such that the trajectory leaving $(0,0)$ now tends to the anterior mesendoderm steady state: (*iii*) is a blow up of the region in the box in (*i*). (*iv*) Trajectories from the origin for various A . The amount of time that the system remains close to the unstable state increases as A approaches A^{c}; for $A = A^{\mathrm{c}}$ (in this case $A^{\mathrm{c}} \approx 1.72$) the system attains the unstable steady state for all time. **We note that the system is bistable for values of A close to A^{c}.** Parameters were chosen as in Table 2.

anterior mesendoderm steady states for $A < A^{\mathrm{c}}$ and $A > A^{\mathrm{c}}$, respectively. Solutions for A near A^{c} pass through a 'mesendoderm' phase in which both M and B lie close to the stable manifold of the saddle point. As they approach the saddle, they diverge from this stable manifold and subsequently tend to the appropriate stable steady state. These solutions are likely to be sensitive to noise, and such regimes warrant further investigation.

4. The *in-vivo* model

In this Section we consider solutions to the *in-vivo* model (10)-(12).

4.1. Steady-state analysis

The steady states to the *in-vivo* model (10)-(12) are determined by first solving (17) for N^*:

$$V^* = C^* = 0, \qquad N^* = \psi \mathcal{H}\left(\frac{N^*}{\theta_{N,N}}\right), \tag{17}$$

where $\psi = \lambda_{N,N}/\mu_N$. The second of

$$I^* = 0, \qquad L^* = \frac{\lambda_{N,L}}{\mu_L}\mathcal{H}\left(N^*\right), \tag{18}$$

then gives L^*, and the coupled system

$$E^* = \frac{\lambda_{B,E}}{\mu_E}\mathcal{H}\left(B^*\right), \tag{19a}$$

$$B^* = \left\{\frac{\lambda_{E,B}}{\mu_B}\mathcal{H}\left(E^*\right) + \frac{\lambda_{N,B}}{\mu_B}\mathcal{H}\left(N^*\right)\right\}\left\{1 - \mathcal{H}\left(G^* + M^*\right)\right\}, \tag{19b}$$

$$G^* = \frac{\lambda_{M,G}}{\mu_G}\mathcal{H}\left(\frac{M^*}{\theta_{M,G}}\right)\left\{1 - \mathcal{H}\left(\frac{G^*}{\theta_{G,G}}\right)\right\}, \tag{19c}$$

$$M^* = \frac{\lambda_{A,N}}{\mu_M}\mathcal{H}\left(\frac{N^*}{\theta_{N,M}}\right)\left\{1 - \mathcal{H}\left(\frac{B^*}{\theta_{B,M}}\right)\right\}. \tag{19d}$$

can then be solved for E^*, B^*, G^* and M^* in terms of N^* (for $\lambda_{B,E} = 0$, $E^* = 0$, solutions to (19) are equivalent to the steady states of (9) if we identify A with N^*) . It follows from our numerical investigations of the steady states to (9) (see Section 3.1) that the *in-vivo* model has stable steady states corresponding to mesoderm and anterior mesendoderm. We note that (17)-(19) are independent of the levels of VegT (V) and β-Catenin (C) since these decay to zero as a steady state is approached. However, in Section 4.2 we show that the initial concentrations of VegT (V_0) and β-Catenin (C_0) can determine whether the *in-vivo* model (10)-(12) evolves to the mesoderm

Figure 10: (i)-(ii) Steady-state solutions to (19) for $N^* = 0$ (blue curves) and $N^* > 0$ (black curves) for Brachyury (B^*), Mix (M^*), Goosecoid (G^*) and eFGF (E^*) plotted against $\lambda_{E,B}$. The thick and thin solid lines are stable branches, and can be interpreted as mesoderm and anterior mesendoderm respectively. The dashed lines are unstable branches. Thus, there are two 'mesoderm' steady states, one of which corresponds to upregulation of *Brachyury* by eFGF in the absence of Nodal (blue line) and the other to its upregulation by Nodal and eFGF. Parameter values were chosen as in Table 2.

or the anterior mesendoderm steady state. Furthermore, we recall that the *in-vivo* model is of a single cell embedded in a population of identical cells, which allows us to include *eFGF* and *Nodal* autoregulation reflected in the $\lambda_{B,E} > 0$ and $\lambda_{N,N} > 0$ terms in (17) and (19). It can be easily shown that (17) can be bistable (depending on parameter choices) with stable steady states $N = 0$ and $N = N^*$ with $N^* > 0$ (corresponding to downregulated and upregulated *Nodal* respectively). In turn, (19) is itself bistable for both $N = 0$ and $N = N^*$, with the latter case corresponding closely to the *in-vitro* steady states (*i.e.* one to mesoderm and the other to anterior mesendoderm) and the former corresponding to *eFGF* and *Brachyury* upregulating the other (*i.e.* mesoderm) or the trivial steady state.

The appearance of the eFGF-dependent mesoderm steady-state is supported with the following experimental observations. bFGF signalling (which acts through the same signal transduction pathway as eFGF) can maintain *Brachyury* expression in the absence of Activin-like (*i.e.* Nodal) signalling (Schulte-Merker and Smith (1995)). Furthermore, Nodal levels appear to be significantly lower in the marginal region than in the vegetal region from stage 10 (9 hours after fertilisation) onwards (Schohl and Fagotto (2002)), when a ring of eFGF and Brachyury expression can be detected (Schohl and Fagotto (2002); Lemaire et al. (1998)). In addition, *Brachyury* expression becomes dependent on cell-cell communication only after stage 9 (7 hours after fertilisation) (Schulte-Merker and Smith (1995); Yasuo and Lemaire (1999)). Taken together, these data suggest that marginal zone cells approach the eFGF-dependent mesoderm steady state in stage 10 embryos. At earlier times, however, when marginal zone cells are exposed to higher levels of Nodal signalling, cells may approach the Nodal-dependent mesoderm steady-state. Representative examples of the two mesoderm steady-states are provided in Figure 10.

4.2. Time-dependent solutions to the in-vivo model

In this subsection we investigate these issues further by investigating time-dependent solutions to the *in-vivo* model (10)-(12).

4.2.1. Numerical investigation

To compare the *in-vivo* model to the experimental observations noted above, we set initial conditions (7) with $V_0 \geq 0$ and $C_0 \geq 0$ and first solve (10) numerically: see Figure 11 for representative solutions. *Nodal* expression is transient in disaggregated cells injected with VegT (Clements et al. (1999)). This corresponds to setting $\psi = 0$, and the model predicts that N will tend to zero. However, *Nodal* expression is strongly detected in whole animal caps injected with VegT (Clements et al. (1999)). With regard to the model, this corresponds to setting $\psi > 0$ and V_0 to be sufficiently large that N evolves to the nontrivial stable steady state N^* (see Figure 11). Numerical investigations suggest that solutions to (10) will typically overshoot N^*, the extent of the overshoot varying according to initial conditions V_0, C_0 Comparison of $C_0 = 0$ and $C_0 > 0$ solutions reveals that increasing the β-Catenin concentration causes that of Nodal (N) to grow to high levels before N evolves to N^*. We note that this overshoot is consistent with the observation that Nodal expression levels appear higher in β-Catenin positive cells than in negative ones, and that these levels steadily decrease (Agius et al. (2000); Lee et al. (2001); Schohl and Fagotto (2002)).

Figure 11: Numerical solutions to (10) with initial conditions (7) and with $N_0 = 0$ and C_0, V_0 are as indicated. For V_0 sufficiently large, N tends to N^*, typically first overshooting it; choosing $C_0 > 0$ can typically increase the level of overshoot. The remaining parameters were chosen as in Table 2.

Figure 12: Numerical solutions to the *in-vivo* model (10)-(12) plotted against V_0 at various times τ. (i) In the absence of β-Catenin, VegT can induce a differential response in Brachyury (thin solid line), eFGF (dotted line) and Mix (dashed line), Goosecoid (dash-dotted line) expression levels. Nodal (thick blue solid line) expression is monotonic in V_0. (ii) The presence of a β-Catenin gradient (see text) causes the system to evolve to the mesoderm steady state for lower V_0. N expression is now non-monotonic in V_0, and initially appears highest for $V_0 < 5$. (iii) Diagram indicating the steady-states to which the system evolves, depending on the initial levels of VegT (V_0) and β-Catenin (C_0). Parameters were chosen as in Table 2.

We now study the effect of VegT on the dynamics of the full *in-vivo* model, initially in the absence of β-Catenin (*i.e.* with $C_0 = 0$). Thus, we solve (10)-(12) numerically with $C_0 = 0$ for various V_0. Representative solutions are plotted against V_0 in Figure 12(i). We note that both *Brachyury* and *Mix* are activated by VegT. Simulations suggest that, provided parameters are chosen appropriately, V_0 can determine cell fate: if V_0 is sufficiently small then the system will evolve to the mesoderm branch; increasing V_0 beyond some critical value (V_0^c) causes the system to evolve to the anterior mesendoderm steady state (see Figure 12(i) for $\tau = 8$). If V_0 is too small then the system will evolve to the trivial steady state. The VegT dose response experiments of Clements et al. (1999); Kavka and Green (2000) follow a similar trend. Unfortunately, however, a direct comparison with the Mix and Brachyury expression levels from these experiments is not possible, and the response of these two genes two VegT warrants further investigation.

To gain some insight into how β-Catenin may affect cell fate, we choose initial conditions (7) to (10)-(12) so that the *in-vivo* model mimics the spatial structure of an embryo (noting that there is no communication between cells in this model). Thus the initial concentration profiles of VegT (V_0) and β-Catenin (C_0) are chosen to correspond to a line of cells that run from the presumptive dorsal mesoderm (where VegT deposits are low and β-Catenin is expressed) to the presumptive anterior mesendoderm (where VegT deposits are highest and β-Catenin is low) as illustrated in Figure 1(ii). Thus, there is a negative gradient of β-Catenin (C_0) protein that overlaps a positive gradient of VegT (V_0) protein; specifically we take $C_0 = a - bV_0$ for $V_0 < a/b$ and $C_0 = 0$ for $V_0 \geq a/b$, representative numerical solutions being shown in Figure 12(ii) for $a = 50$, $b = 10$. In comparison to the case $C_0 = 0$, *Nodal* expression levels are initially highest in β-Catenin positive (*i.e.* marginal-zone) cells, which form the presumptive mesoderm, as is detected experimentally (Isaacs et al. (1995); Schohl and Fagotto (2002)). Furthermore, solutions for low V_0 now evolve to the mesoderm steady state instead of the trivial one (compare Figure 12(i) to 12(ii) for $\tau = 8$). Thus, the range of VegT concentrations that can induce mesoderm increases in the presence of β-Catenin (see Figure 12(iii)). This observation leads to the prediction that, in embryos depleted of β-Catenin, the expression domain of *Brachyury* that forms in the equatorial zone will appear reduced in size. Furthermore, upon comparing Figures 12(i) and 12(ii) for $\tau = 8$, we note that Brachyury expression is delayed in β-Catenin negative cells (when compared to β-Catenin positive cells), which has been observed experimentally (Schohl and Fagotto (2003)).

Numerical solutions of the *in-vivo* model, presented in Figure 13, suggest that the early time behaviour of solutions is governed largely by the VegT response, which determines whether Mix dominates Brachyury or vice versa. As time increases, the concentration of Nodal (N) grows and reinforces the expression level of the dominant factor (Mix or Brachyury), ultimately causing solutions to commit to either the mesoderm or anterior mesendoderm steady states. We discuss this further in Section 5.

Figure 13: Nodal appear to largely reinforce the VegT pre-pattern. A comparison between solutions to (10)-(12) in the presence ($\lambda_{V,N} = 1$, solid lines) and absence ($\lambda_{V,N} = 0$, dashed lines) of Nodal (*i.e.* $N \equiv 0$ for $\lambda_{V,N} = 0$) for $V_0 = 2.8$ and $C_0 = 0$. Parameter values were chosen as in Table 2

5. Discussion

In this paper we developed a model for simplifications of the **dorsal** mesendoderm network presented in Loose and Patient (2004) designed to describe aspects of *in-vivo* and of *in-vitro* behaviour (see Figures 2 and 3). Both versions of the model were found to be bistable, with stable steady states corresponding to dorsal mesoderm (*i.e.* to *Brachyury* expressing cells) and anterior mesendoderm (*i.e.* to *Mix* and *Goosecoid* co-expressing cells).

The *in-vitro* model is able to reproduce qualitatively the quantitative single cell Activin dose response of Gurdon et al. (1999); Papin and Smith (2000) (see Figure 6). In both the experiments and the model, *Goosecoid* and *Brachyury* are co-expressed in cells for a wide range of Activin concentrations. These expression profiles are subsequently refined, until *Brachyury* is expressed only in cells treated with a low concentration of Activin, with *Goosecoid* being expressed instead in cells with a high concentration. Furthermore, whole tissue experiments indicate that *Mix.1* is expressed in cells that receive a high concentration of Activin and that its expression domain overlaps that of *Goosecoid* (Gurdon et al. (1996)).

Our numerical investigations of the *in-vivo* model suggest that the initial concentration of VegT can determine cell fate in a similar fashion to Activin, which is consistent with dose response experiments of Clements et al. (1999); Kavka and Green (2000). Our single-cell model allows us to make the following inferences about the spatial patterning of *Xenopus* embryos. We recall from Section 1.2 that there exists a putative gradient of VegT that lies between the presumptive endoderm and the presumptive mesoderm (illustrated in Figure 1(*ii*)). Anterior mesendoderm (cells co-expressing *Goosecoid* and *Mix*) will form in dorsal cells receiving the highest concentration of VegT, whereas mesoderm will form where VegT concentrations are lower (see Figure 1). Thus, to summarise, our model results suggest that in normal embryos, dorsal cells will initially co-express *Goosecoid*, *Mix.1* and *Brachury*. Cells at the vegetal end will have negligible levels of *Brachyury* and high levels of *Mix.1* and *Goosecoid*, whereas cells at the dorsal end of the marginal zone will have low levels of *Mix.1* and *Goosecoid*, and high lives of *Brachyury*. Between these two extremes will a be a population of mesendodermal cells that transiently express all three factors (Lemaire et al. (1998); Latinkic and Smith (1999); Wardle and Smith (2004)) (see Figure 1(*i*)). The mesendoderm will differentiate to form two separate cell populations, one representing mesoderm in the marginal zone and the other anterior mesendoderm in the dorsal vegetal region. This is consistent with the experimentally-observed expression profiles of *Goosecoid*, *Mix.1* and *Brachury* (see Figure 1). **Importantly, this role for VegT in the spatial patterning of mesoderm and anterior mesendoderm is entirely consistent with the VegT depletion experiments of Zhang et al. (1998) (see Section 1.2 for further details)**.

As noted in Section 1, at present it is not clear whether in practice dorsal vegetal cells co-expressing *Goosecoid* and *Mix* segregate. Disruption of either *Goosecoid* or *Mix.1* function can cause defects in anterior (head) development (Latinkic and Smith (1999); Yao and Kessler (2001)). In addition, injection of *Goosecoid* mRNA into ventral tissues leads to the formation of secondary head structures (Cho et al. (1991)). We note that since *Mix.1* is expressed ventrally, the second obervation is entirely consistent with the first. Thus, *Goosecoid* may require the presence of *Mix.1* to initiate development of anterior structures. However, this co-expression is transient: current evidence suggests that, unlike *Goosecoid*, *Mix.1* expression has entirely disappeared by stage 13[4] (Wardle and Smith (2004)). As already noted, *Goosecoid* is associated with mesoderm and *Mix.1*

[4]Stage 13 broadly corresponds to the end of gastrulation

with endoderm. Thus, between stages 10 and 13 it is possible that the co-expressing cells may form two distinct cell populations, each expressing one of the two markers. However, our results suggest that a negative feedback loop between *Mix* and *Goosecoid* would be required to drive this separation, and this has not yet been identified either *in vivo* or *in vitro*.

Goosecoid expression is absent from the ventral region of the embryo, which is inhibited by ventrally-expressed antagonists such as Vent-1 and Vent-2 (also known as Xom, Vox or Tbr-1) (Sander et al. (2007)). In turn, *Vent-1 and Vent-2* expression is antagonised by Goosecoid (Sander et al. (2007); Onichtchouk et al. (1996); Gawantka et al. (1995)). Thus, *Vent-1/2* and *Goosecoid* are able to interact in a cross inhibitory loop. This aspect of embryo development has been modelled in Saka, Y. and Smith, J.C. (2007). Depletion of *Vent-1/2* leads to the dorsalisation of the embryo, so that *Goosecoid* is expressed throughout the vegetal region (Sander et al. (2007)) and its expression completely overlaps that of *Mix.1* (Lemaire et al. (1998)) (see Figure 1). In the absence of *Goosecoid* our model can evolve to steady states corresponding to ventral mesoderm or endoderm (see below for a further discussion). These data indicate that if we do include *Vent-1/2* in our model, it may also be able to account for mesendoderm differentiation on the ventral side of embryo.

The analysis of our reduced *in-vitro* model (see Section 3.3) suggests that the mesendoderm phase is characterised by solutions passing close to the stable manifold of the unstable steady state. Moreover, the sharp transition between the two cell fates in response to increasing Activin (A) corresponds to a shift in the basins of attraction for the mesoderm and anterior mesendoderm steady states (whereby the separatrix crosses the phase plane origin at the critical values $A = A^{\mathrm{c}}$) (see also Middleton et al. (2003)). For $A = A^{\mathrm{c}}$, a trajectory will pass through the origin and move along the stable manifold and enter the 'mesendoderm' steady state. This would suggest that the mesendoderm phase will persist longer the closer the level of Activin (A) is to this critical value (A^{c}). A similarly critical level of VegT exists for the *in-vivo* model. Solutions passing through this phase will be sensitive to perturbations and this will be important in what follows. Thus, our *in-vitro* model suggests that *in vivo* the mesendoderm could act as a malleable population of cells that sits between the mesoderm and endoderm cell populations. We hypothesise that, *in-vivo*, this allows the embryo to refine gradually the border between the two cell populations until it is 'precise'. Part of this refinement process could come through an initial response of the mesendodermal cell population to the VegT gradient (see above), followed by a further refinement mediated by a Nodal signalling gradient (which does not itself form until stage 10.5, 11 hours after fertilisation (Schohl and Fagotto (2003))). In addition, our single cell model results indicate that the Nodal signals represent a secondary gradient that is more refined than the initial VegT gradient (which is likely to be rather imprecise (Clements, D. and Woodland, H.R. (2003); Dale and Slack (1987))). This refinement process is due in large part to the *Nodal* positive feedback loop that reinforces high, but not low, VegT inputs. The formation of the Nodal gradient will be the subject of a subsequent paper.

Despite the above observations, our numerical investigations of the *in-vivo* model indicate that the Nodal signals simply reinforce the VegT and β-Catenin prepattern. As we now argue, this suggests the presence of additional mechanisms missing from our simplified network. In the model, the duration of the mesendoderm phase plays a large role in how the VegT and Nodal signalling gradients interact. In reality, the mesendoderm can be detected between stages 10 and 11, corresponding to a duration of approximately 2-3 hours (Lemaire et al. (1998)). In the model, this would correspond to choosing the level of VegT to be unrealistically close to its critical value. Furthermore, this level of VegT would have to be attained by most cells in the mesendoderm population, which seems particularly unlikely. Consistent with this, our investigations with a multicellular version of the *in-vivo* model (Middleton, A. (2007)) have revealed the mesendoderm to occupy only a couple of cells for a brief period of time, contrary to experimental observation. It is quite possible that additional interactions, not present in our simplified version of the GRN, could maintain the mesendoderm by keeping trajectories close to the unstable manifold (*i.e.* so it is metastable). In the model, the duration of the mesendoderm phase is reduced in part by the influence of Nodal. This

can be explained as follows. We have assumed that cells are simultaneously responsive to VegT, β-Catenin and Nodal. Exposing cells to Nodal whilst they respond to VegT and β-Catenin can be interpreted as a perturbation of the system in which trajectories are pushed away from the unstable manifold. This causes trajectories to evolve to one of the stable steady states, corresponding to the differentiation of a cell. As we now discuss, a cell's capacity to respond to either VegT or Nodal signals appears to be depend on its developmental age, and this could have important consequences for the duration of the mesendoderm phase.

There is a growing body of evidence which suggests that mesoderm and anterior-mesendoderm formation is a two step process (Yasuo and Lemaire (1999); Clements, D. and Woodland, H.R. (2003); Clements et al. (1999); Kavka and Green (2000)). The first phase (approximately stages 2^5 to 9^6) are associated with cell-autonomous[7] activation of early mesoderm and anterior-mesendoderm association genes, which is mediated in large part by maternal factors such as VegT (Yasuo and Lemaire (1999); Clements, D. and Woodland, H.R. (2003); Clements et al. (1999); Kavka and Green (2000)) (**during which, we predict, an initial expression pattern of *Brachyury*, *Mix* and *Goosecoid* begins to emerge, see above for details**). In the secondary phase (stage 9 onwards), cells are largely dependent on cell-cell communication, with this communication largely being mediated by members of Nodal family of signals (Yasuo and Lemaire (1999); Clements, D. and Woodland, H.R. (2003); Clements et al. (1999); Kavka and Green (2000)) (**through which, we predict, the expression patterns of the key mesendoderm genes are gradually refined, see above for details**). The switch from cell-autonomous to cell non-autonomous[8] induction of mesoderm and anterior-mesendoderm genes is indicated by the following experimental observations. First, VegT appears to activate a self-limiting mechanism that prevents it from activating downstream target genes such as *Mix.1* after stage 10 (Clements, D. and Woodland, H.R. (2003)). Second, the competence of cells to respond to Activin-like signals (such as Nodal) appears to be highly regulated. *In-vitro* experiments indicate that Activin can only activate downstream genes such as *Goosecoid* and *Brachyury* from stage 9 onwards (Saka, Y. and Smith, J.C. (2007); Bourillot et al. (2002)) in animal caps[9], regardless of the time at which the cells are exposed to the signal (Saka, Y. and Hagemann, A.I. and Piepenburg, O. and Smith, J.C. (2007)). Consistent with this, activated Smad complexes, which mediate Activin-like signals (including members of the Nodal family), are prevented from entering the nucleus until after stage 8[10] in animal caps (Saka, Y. and Hagemann, A.I. and Piepenburg, O. and Smith, J.C. (2007)). This may also explain why *in-vivo* activated Smad complexes are not detected in the animal pole (where ectoderm normally forms) until stage 8.5 and in the vegetal/dorsal pole (where mesoderm and anterior mesendoderm normally form) until stage 9 (Schohl and Fagotto (2002)), even through *Nodal* genes appear to be expressed from stage 8 onwards (Yasuo and Lemaire (1999)). Thus, one mechanism for controlling the duration of the mesendoderm phase may be to regulate the time at which cells have the capacity to respond to a Nodal signal.

The above comments lead us to recall that *Xenopus* has six representatives of the Nodal signalling family rather than the ancestral single copy. Members of the Nodal family can be regulated by TGF-β signalling activity, resulting in complex feedback loops between Nodals. We speculate that these feedback mechanisms may contribute to the establishment of a precise signalling gradient more rapidly than can be achieved by a single Nodal. Thus we suggest that the simplification process we have used to generate this network omits interactions that contribute to the overall robustness of the network measured in terms of the speed at which the gradient is established and the ability of the network to establish the same gradient in response to different starting conditions. If so, this may link the number of Nodal genes to the rate at which *Xenopus* can develop, which is fast compared

[5]Stage 2 corresponds to the first cleavage
[6]Stage 9 occurs 7 hours after fertilisation of the egg
[7]In cell-autonomous regulation the responding cell is the source of the inducing factor
[8]In cell non-autonomous regulation the source of the signal is not the responding cell
[9]An animal cap is explant cut from the animal pole of the embryo, where ectoderm normally forms, see Figure 1
[10]Stage 8 marks the onset of the mid-blastula transition, prior to which gene transcription cannot typically ccur

to other amphibians.

Acknowledgements

This work was supported by the Engineering and Sciences Research Council.

References

Agius, E., Oelgeschlager, M., Wessely, O., Kemp, C., De Robertis, E., 2000. Endodermal Nodal-related signals and mesoderm induction in *Xenopus*. Development 127, 1173–1183.

Alberts, B., Bray, D., Lewis, J., Raff, M., Roberts, K., Watson, J., 1994. Molecular biology of the cell, Third Edition. Garland Publishing, Inc.

Alon, U., 2007. An Introduction to Systems Biology: Design Principles of Biological Circuits. Chapman & Hall/CRC.

Artinger, M., Blitz, I., Inoue, K., Tran, U., Cho, K., 1997. Interaction of *goosecoid* and *brachyury* in Xenopus mesoderm patterning. Mech Dev 65 (1-2), 187–96.

Becskei, A., Seraphin, B., Serrano, L., 2001. Positive feedback in eukaryotic gene networks: cell differentiation by graded to binary response conversion. EMBO J. 20, 2528–35.

Bourillot, P., Garrett, N., Gurdon, J., 2002. A changing morphogen gradient is interpreted by continuous transduction flow. Development 129, 2167–2180.

Cho, K., Blumberg, B., Steinbeisser, H., De Robertis, E., 1991. Molecular nature of Spemanns organizer: the role of the Xenopus homeobox gene goosecoid. Cell 67 (6), 1111–1120.

Cinquin, O., Demongeot, J., 2002. Roles of positive and negative feedback in biological systems. C. R. Biol. 325, 1085–95.

Clements, D., Friday, R., Woodland, H., 1999. Mode of action of VegT in mesoderm and endoderm formation. Development 126, 4903–4911.

Clements, D. and Woodland, H.R., 2003. VegT induces endoderm by a self-limiting mechanism and by changing the competence of cells to respond to TGF-beta signals. Dev Biol. 258, 454–63.

Dale, L., Slack, J., 1987. Fate map for the 32-cell stage of Xenopus laevis. Development 99, 527–551.

Davidson, E., Rast, J., Oliveri, P., Ransick, A., Calestani, C., Yuh, C., Minokawa, T., Amore, G., Hinman, V., Arenas-Mena, C., Otim, O., Brown, C., Livi, C., Lee, P., Revilla, R., Rust, A., Pan, Z., Schilstra, M., Clarke, P., Arnone, M., Rowen, L., Cameron, R., McClay, D., Hood, L., Bolouri, H., 2002. A genomic regulatory network for development. Science 295, 1669–1678.

Dyson, S., Gurdon, J., 1998. The interpretation of position in a morphogen gradient as revealed by occupancy of Activin receptors. Cell 93, 557–568.

Ermentrout, B., 2002. Simulating, Analyzing, and Animating Dynamical Systems: A Guide to XPPAUT for Researchers and Students. Society for Industrial Mathematics.

Gardner, T., Cantor, C., Collins, J., 2000. Construction of a genetic toggle switch in Escherichia coli. Nature 403, 339–42.

Gawantka, V., Delius, H., Hirschfeld, K., Blumenstock, C., Niehrs, C., 1995. Antagonizing the Spemann organizer: role of the homeobox gene Xvent-1. EMBO J. 14, 6268–79.

Green, J., 2002. Morphogen gradient, positional information, and *Xenopus*: interplay of theory and experiment. Dev. Dyn. 225, 392–408.

Green, J., Smith, J., Gerhart, J., 1994. Slow emergence of a multithreshold response to Activin requires cell dependent sharpening but not prepattern. Development 120, 2271–2278.

Guo, W., Chan, A., Liang, H., Wieder, E., Molldrem, J., Etkin, L., Nagarajan, L., 2002. A human Mix-like homeobox gene MIXL shows functional similarity to *Xenopus* Mix.1. Blood 100, 89–95.

Gurdon, J., Harger, P., Mitchell, A., Lemaire, P., 1994. Activin signalling and response to a morphogen gradient. Nature 371, 487–492.

Gurdon, J., Mitchell, A., Mahony, D., 1995. Direct and continuous assessment by cells of their position in a morphogen gradient. Nature 376, 520–521.

Gurdon, J., Mitchell, A., Ryan, K., 1996. An experimental system for analyzing response to a morphogen gradient. Proc. Natl Acad. Sci. USA 93, 9334–9338.

Gurdon, J., Standley, H., Dyson, S., Butler, K., Langon, T., Ryan, K., Stennard, F., Shimizu, K., Zorn, A., 1999. Single cells can sense their position in a morphogen gradient. Development 126, 5309–5317.

Hart, A., Hartley, L., Sourris, K., Stadler, E., Li, R., Stanley, E., Tam, P., Elefanty, A., Robb, L., 2002. Mixl1 is required for axial mesendoderm morphogenesis and patterning in the murine embryo. Development 129, 3597–3608.

Heasman, J., 2006. Patterning the early Xenopus embryo. Development 133 (7), 1205–1217.

Huang, S., Eichler, G., Bar-Yam, Y., Ingber, D., 2005. Cell fates as high-dimensional attractor states of a complex gene regulatory network. Phys. Rev. Lett. 94.

Isaacs, H., Pownall, M., Slack, J., 1995. eFGF is expressed in the dorsal midline of *Xenopus laevis*. Int. J. Dev. Biol. 39, 575–579.

Kavka, A., Green, J., 2000. Evidence for dual mechanisms of mesoderm establishment in *Xenopus* embryos. Dev. Dyn. 219, 77–83.

Kerszberg, M., Wolpert, L., 1998. Mechanisms for positional signalling by morphogen transport. J. Theor. Biol. 191, 103–114.

Kofron, M., Demel, T., Xanthos, J., Lohr, J., Sun, B., Sive, H., Osada, S., Wright, C., Wylie, C., Heasman, J., 1999. Mesoderm induction in *Xenopus* is a zygotic event regulated by maternal VegT via TGFbeta growth factors. Development 126, 5759–5770.

Koide, T., Hayata, T., Cho, K., 2005. *Xenopus* as a model system to study transcriptional regulatory networks. Proc. Natl Acad. Sci. USA 102, 4943–4948.

Laslo, P., Spooner, C., Warmflash, A., Lancki, D., H.J., L., Sciammas, R., Gantner, B., Dinner, A., Singh, H., 2006. Multilineage transcriptional priming and determination of alternate hematopoietic cell fates. Cell 126, 755–766.

Latinkic, B., Smith, J., 1999. Goosecoid and Mix.1 repress *Brachyury* expression and are required for head formation in *Xenopus*. Development 126, 1769–1779.

Lee, M., Heasman, J., Whitman, M., 2001. Timing of endogenous Activin-like signals and regional specification of the *Xenopus* embryo. Development 128, 2939–2952.

Lee, T., Rinaldi, N., Robert, F., Odom, D., Bar-Joseph, Z., Gerber, G., Hannett, N., Harbison, C., Thompson, C., Simon, I., Zeitlinger, J., Jennings, E., Murray, H., Gordon, D., Ren, B., Wyrick, J., Tagne, J., Volkert, T., Fraenkel, E., Gifford, D., Young, R., 2002. Transcriptional regulatory networks in saccharomyces cerevisiae. Science 298, 799–804.

Lemaire, P., Darras, S., Caillol, D., Kodjabachian, L., 1998. A role for the vegetally expressed *Xenopus* gene Mix.1 in endoderm formation and in the restriction of mesoderm to the marginal zone. Development 125, 2371–2380.

Lewin, B., 2007. Genes IX. Jones & Bartlett Pub.

Loose, M., Patient, R., 2004. Genetic regulatory networks for mesendoderm: Conserved and evolved features from sea urchins to vertebrates. Dev. Biol. 271, 467–78.

Ma, H., Kumer, B., Ditges, U., Gunzer, F., Buer, J., Zeng, A., 2004. An extended transcriptional regulatory network of escherichia coli and analysis of its hierarchical structure and network motifs. Nucleic Acids Res. 32, 6643–6649.

Mariani, L., Lohning, M., Radbruch, A., Hofer, T., 2004. Transcriptional control networks of cell differentiation insights from helper T lymphocytes. Prog. Biophys. Mol. Biol. 84, 45–76.

Meinhardt, H., 2001. Organizer and axes formation as a self-organizing process. International Journal of Developmental Biology 45 (1; SPI), 177–188.

Middleton, A., King, J., Loose, M., 2003. Qualifying dissertation.

Middleton, A., 2007. Mathematical modelling of gene regulatory networks. PhD Thesis.

Mohn, D., Chen, S., Dias, D., Weinstein, D., Dyer, M., Sahr, K., Ducker, C., Zahradka, E., Keller, G., Zaret, K., Gudas, L., Baron, M., 2003. Mouse Mix gene is activated early during differentiation of ES and F9 stem cells and induces endoderm in frog embryos. Dev. Dyn. 226, 446–459.

Onichtchouk, D., Gawantka, V., Dosch, R., Delius, H., Hirschfeld, K., Blumenstock, C., Niehrs, C., 1996. The Xvent-2 homeobox gene is part of the BMP-4 signalling pathway controlling [correction of controling] dorsoventral patterning of Xenopus mesoderm. Development 122, 3045–53.

Papin, C., Smith, J., 2000. Gradual refinement of Activin-induced thresholds requires protein synthesis. Dev. Biol. 217, 166–177.

Platzer, U., Meinzer, H., 2004. Genetic networks in the early development of caenorhabditis elegans. Int. Rev. Cytol. 234, 47–100.

Rex, M., Hilton, E., Old, R., 2002. Multiple interactions between maternally-activated signalling pathways control *Xenopus* Nodal-related genes. Int. J. Dev. Biol. 46, 217–226.

Roeder, I., Glauche, I., 2006. Towards an understanding of lineage specification in hematopoietic stem cells: A mathematical model for the interaction of transcription factors GATA-1 and PU.1. J. Theor. Biol. 241, 852–865.

Saka, Y. and Hagemann, A.I. and Piepenburg, O. and Smith, J.C., 2007. Nuclear accumulation of Smad complexes occurs only after the midblastula transition in *Xenopus*. Development 134, 4209–4218.

Saka, Y. and Smith, J.C., 2007. A mechanism for the sharp transition of morphogen gradient interpretation in Xenopus. BMC Dev Biol. 7.

Sander, V., Reversade, B., De Robertis, E. M., 2007. The opposing homeobox genes Goosecoid and *Vent1/2* self-regulate Xenopus patterning. The EMBO Journal 26, 29552965.

Schohl, A., Fagotto, F., 2002. Beta-catenin, MAPK and Smad signaling during early *Xenopus* development. Development 129, 37–52.

Schohl, A., Fagotto, F., 2003. A role for maternal beta-catenin in early mesoderm induction in *xenopus*. The EMBO Journal 22, 3303–3313.

Schulte-Merker, S., Smith, J., 1995. Mesoderm formation in response to Brachyury requires FGF signalling. Curr. Biol. 5, 62–67.

Shen-Orr, S., Milo, R., Mangan, S., Alon, U., 2002. Network motifs in the transcriptional regulation network of *Escherichia coli*. Nat. Genet. 31, 64 – 68.

Shimizu, K., Gurdon, J., 1999. A quantitative analysis of signal transduction from Activin receptor to nucleus and its relevance to morphogen gradient interpretation. Proc. Natl Acad. Sci. USA 96, 6791–6976.

Slack, J., 1991. From Egg to Embryo: Second Edition. Cambridge University Press.

von Dassow, G., Meir, E., Munro, E., Odell, G., 1998. Computer simulation of the segment polarity gene network. Dev. Biol. 198.

Wardle, F., Smith, J., 2004. Refinement of gene expression patterns in the early xenopus embryo. Development 131, 4687–96.

Xanthos, J., Kofron, M., Wylie, C., Heasman, J., 2001. Maternal VegT is the initiator of molecular network specifying endoderm in *Xenopus laevis*. Development 128, 167–180.

Yao, J., Kessler, D., 2001. Goosecoid promotes head organizer activity by direct repression of Xwnt8 in Spemann's organizer. Development 128 (15), 2975–2987.

Yasuo, H., Lemaire, P., 1999. A two-step model for the fate determination of presumptive endodermal blastomeres in *Xenopus* embryos. Curr. Biol. 9, 869–879.

Yates, A., Callard, R., Stark, J., 2004. Combining cytokine signalling with T-bet and GATA-3 regulation in Th1 and Th2 differentiation: a model for cellular decision-making. J Theor Biol. 231, 181–96.

Zhang, J., Houston, D., King, M., Payne, C., Wylie, C., Heasman, J., 1998. The role of maternal VegT in establishing the primary germ layers in *Xenopus* embryos. Cell 94, 515–524.

Zhou, X., Sasaki, H., Lowe, L., Hogan, B., Kuehn, M., 1993. Nodal is a novel TGF-beta-like gene expressed in the mouse node during gastrulation. Nature 361, 543–547.

4. Figure 1

Click here to download 4. Figure: Figure1.eps

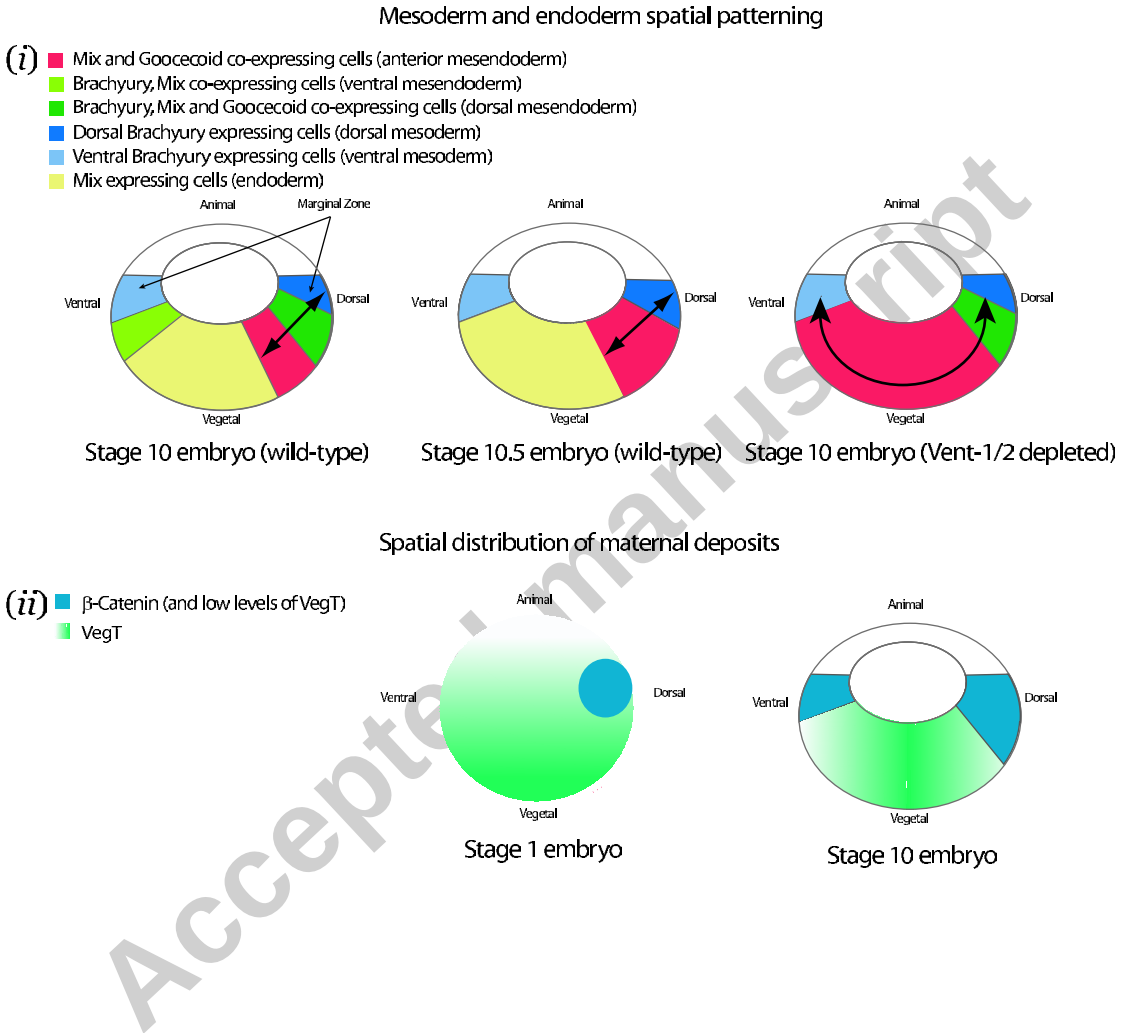

4. Figure 2

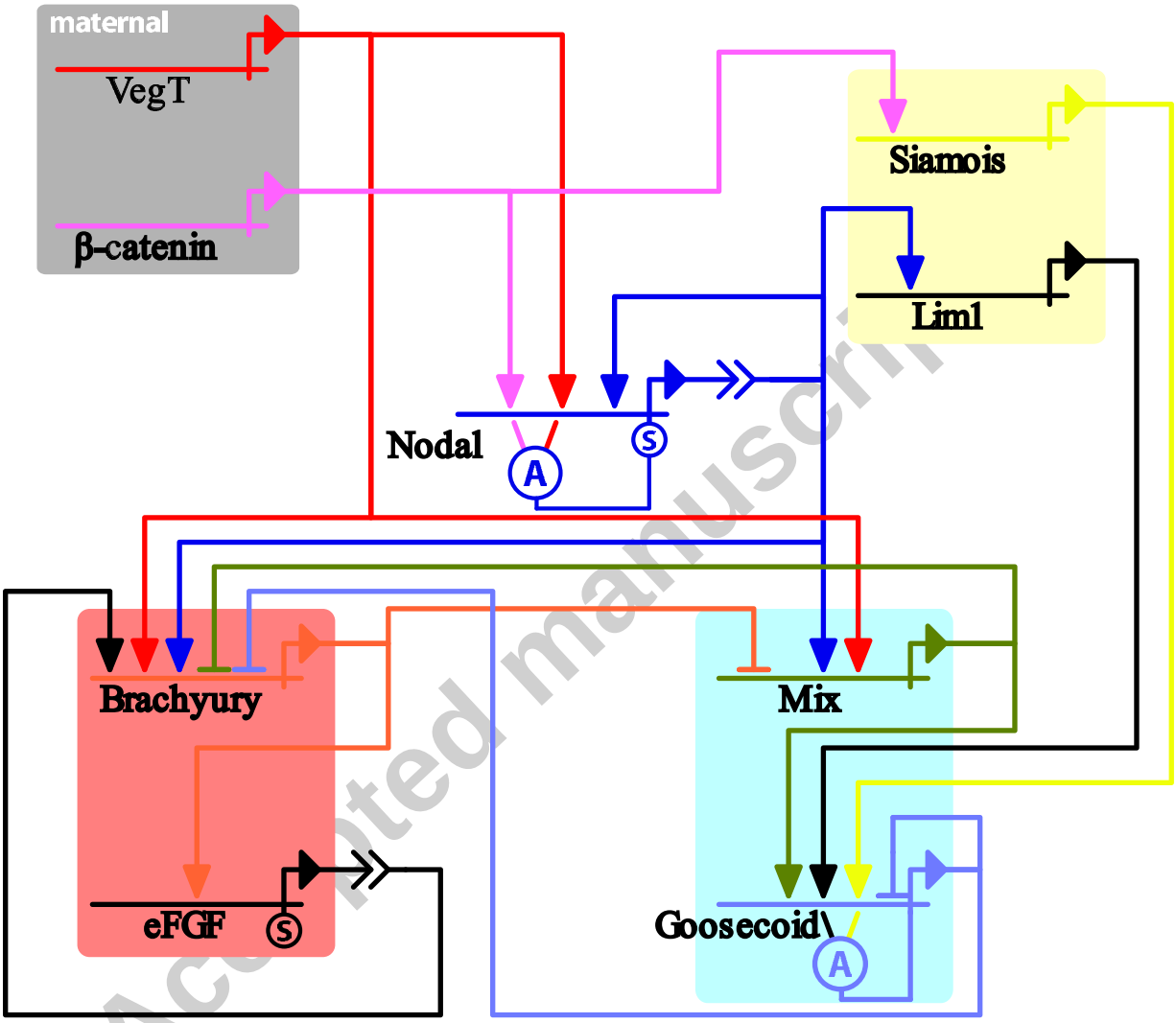

4. Figure 3

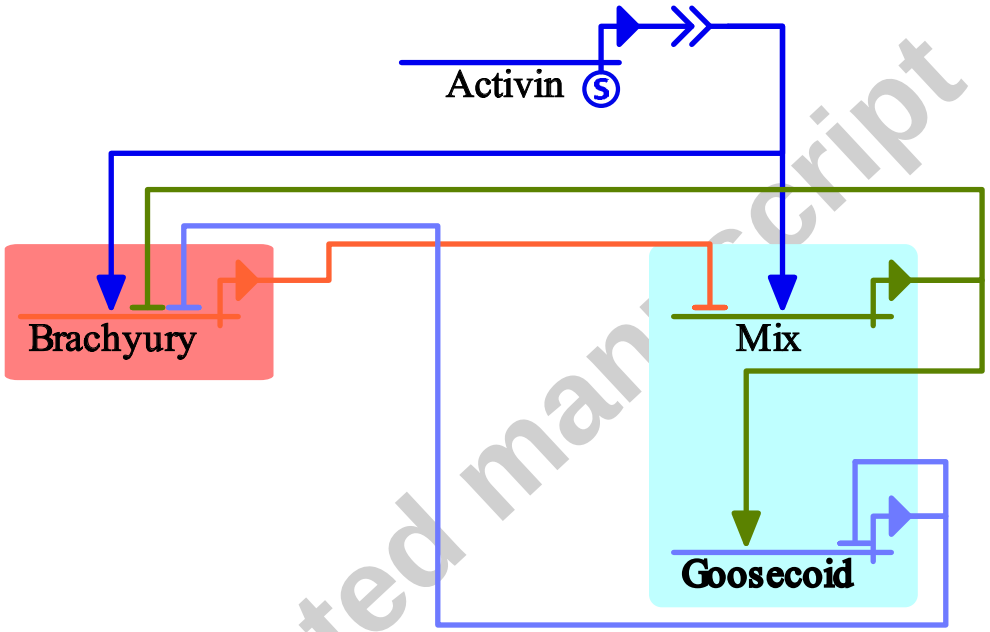

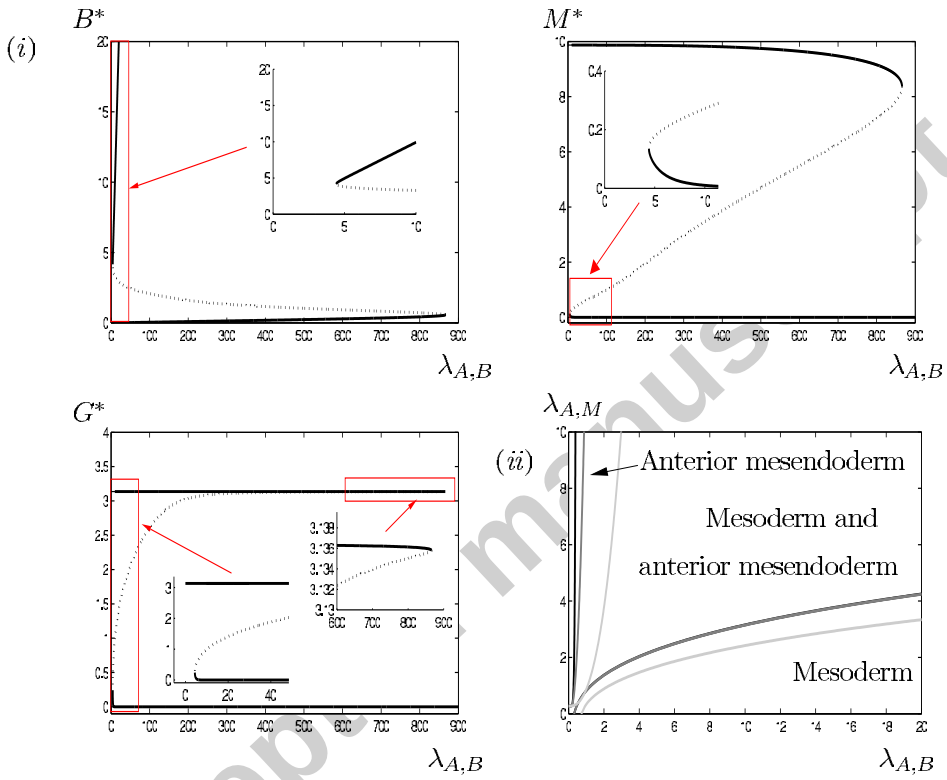

4. Figure 5

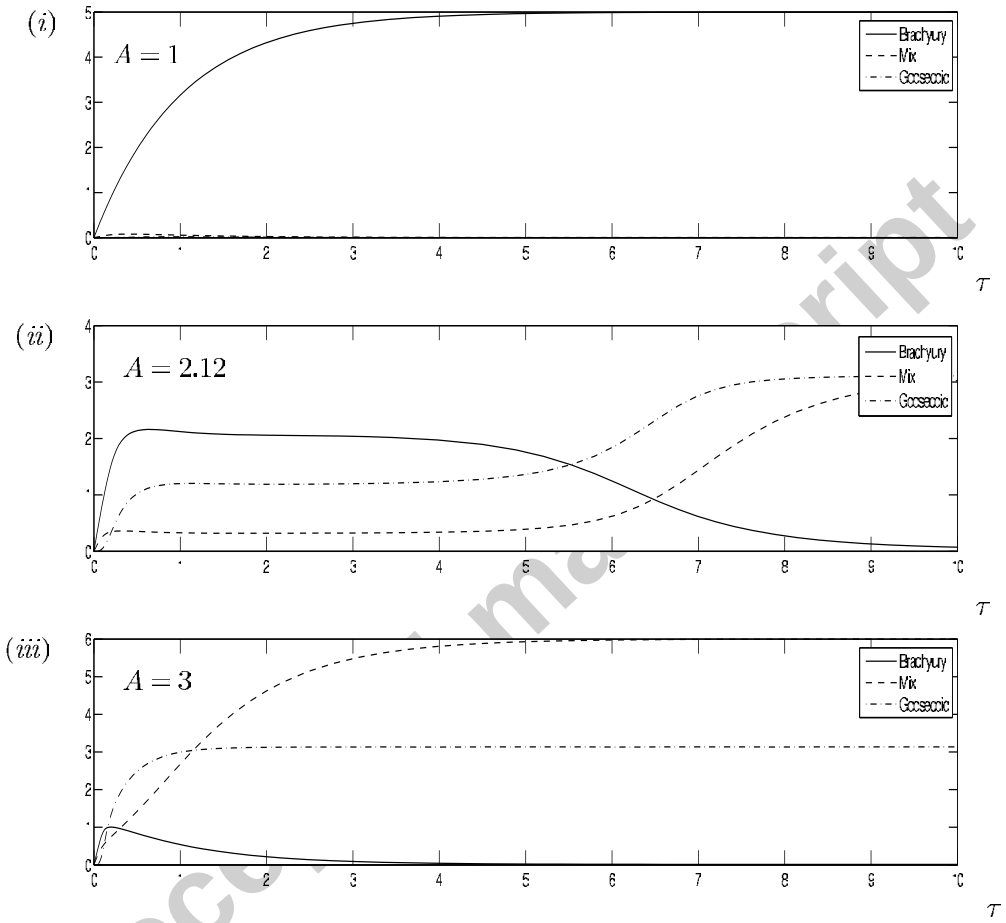

4. Figure 6

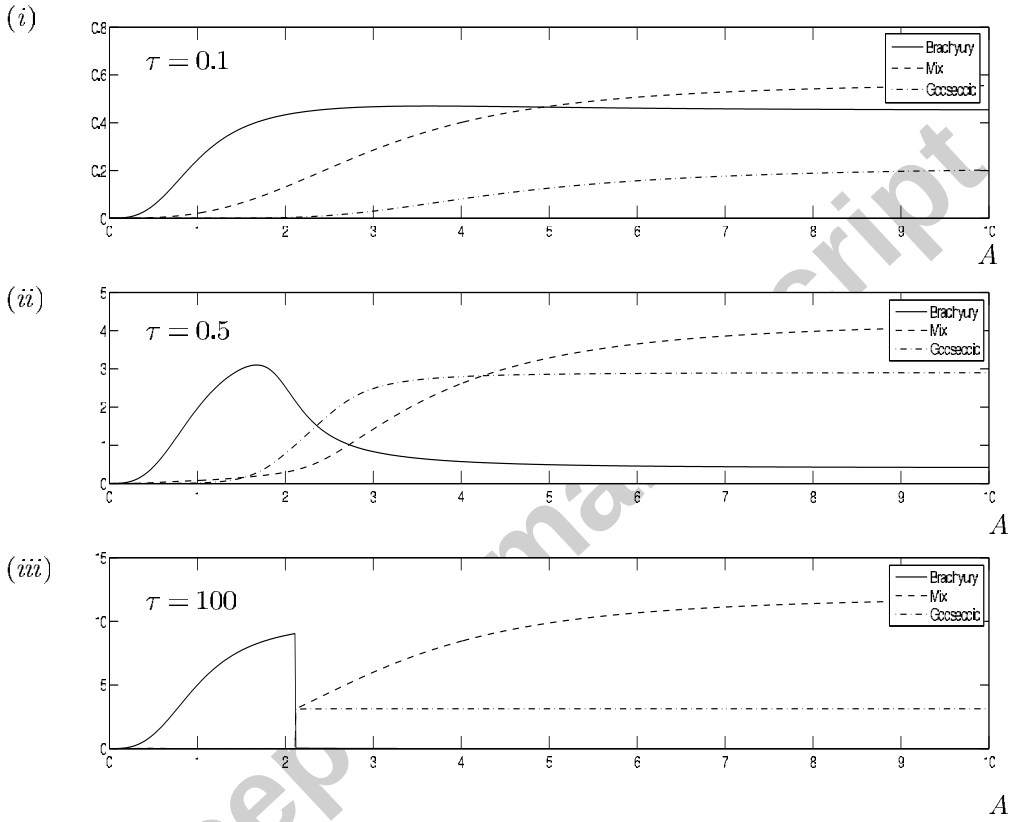

4. Figure 7

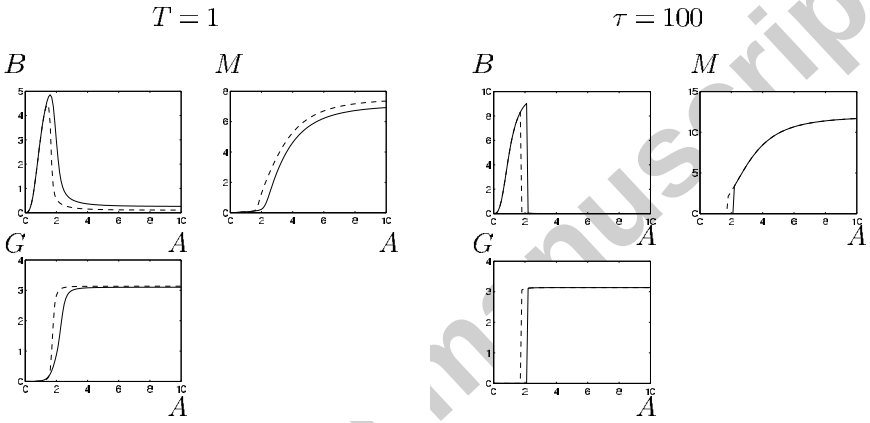

4. Figure 8

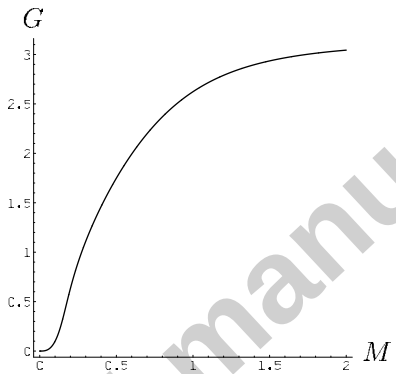

4. Figure 9

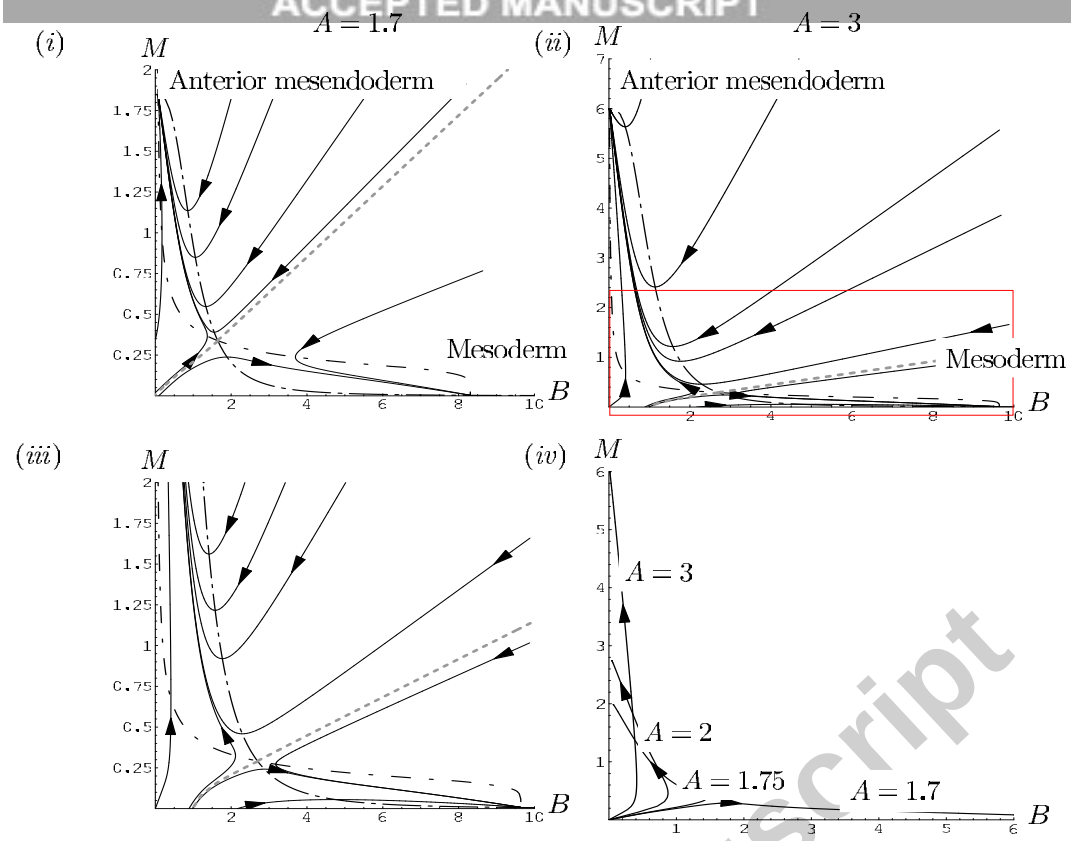

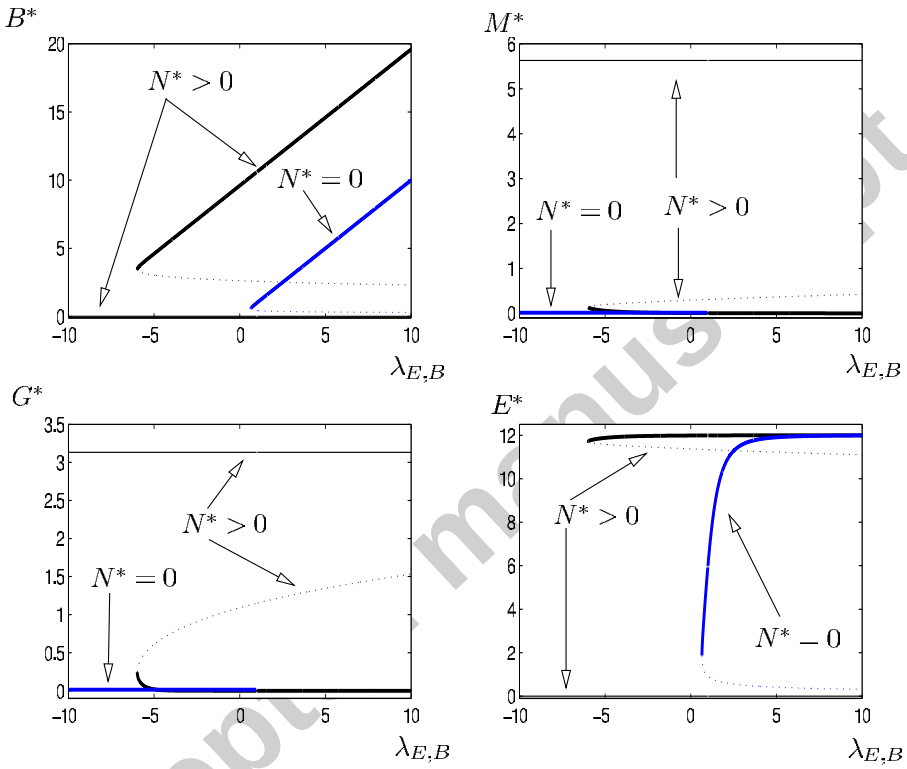

4. Figure 11

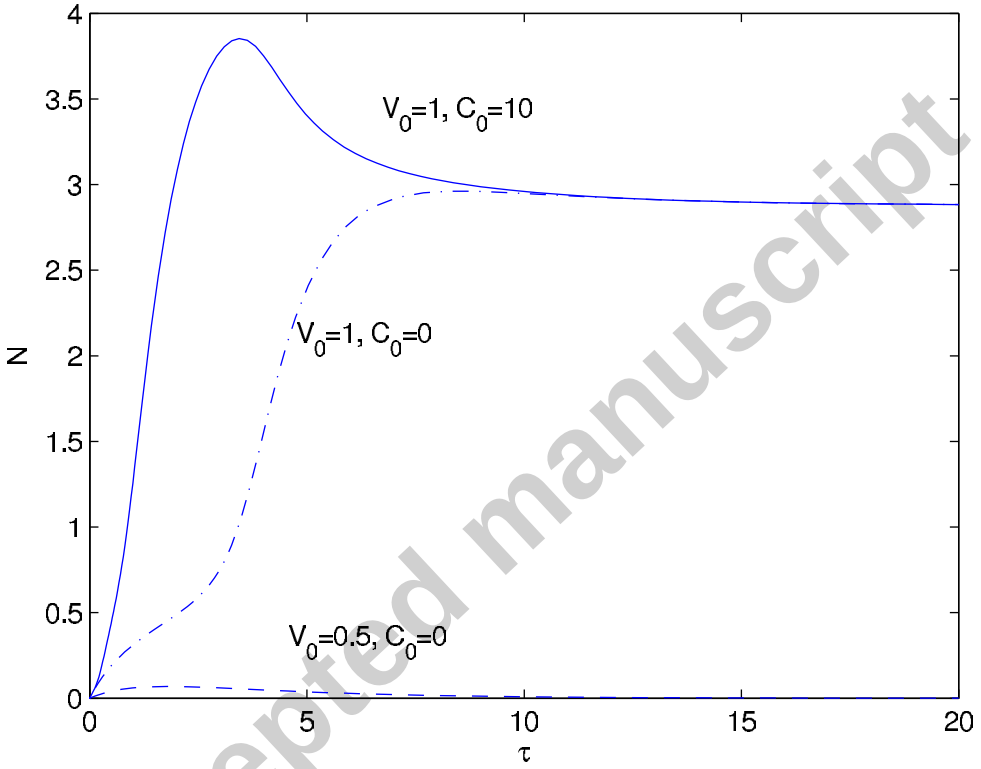

4. Figure 12

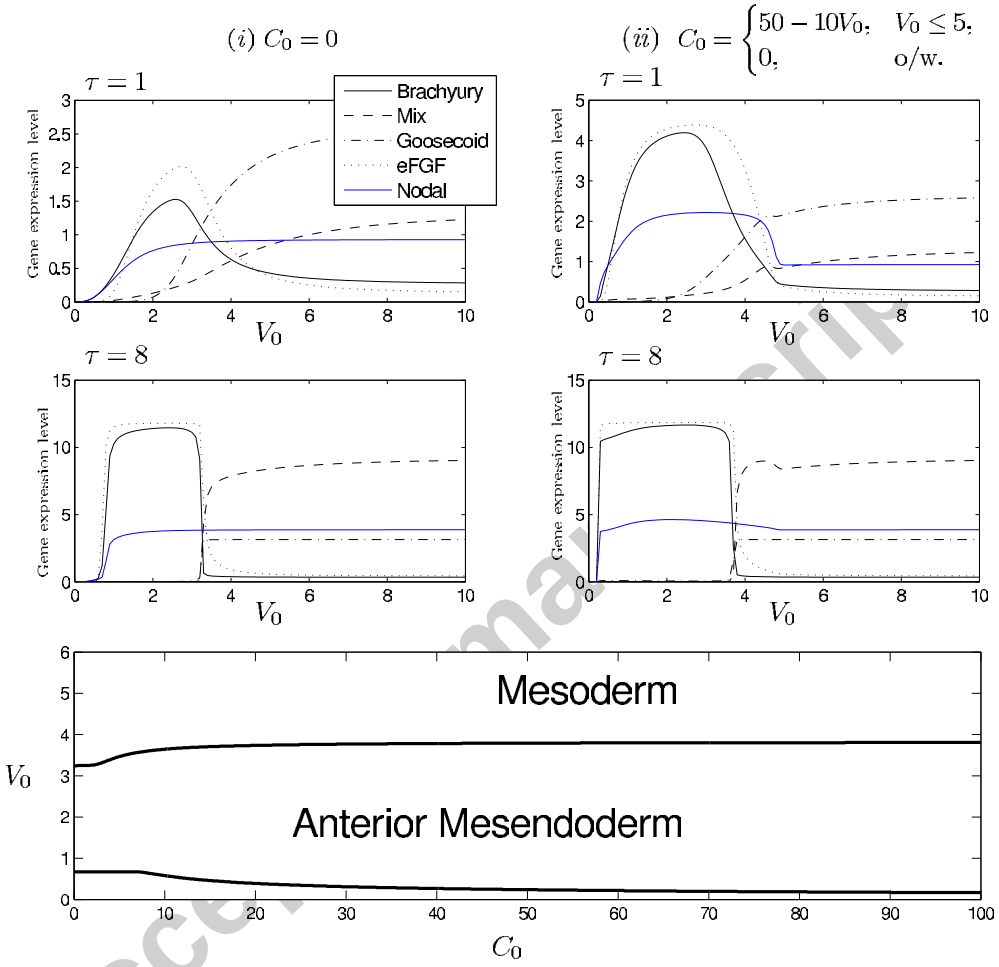

4. Figure 13

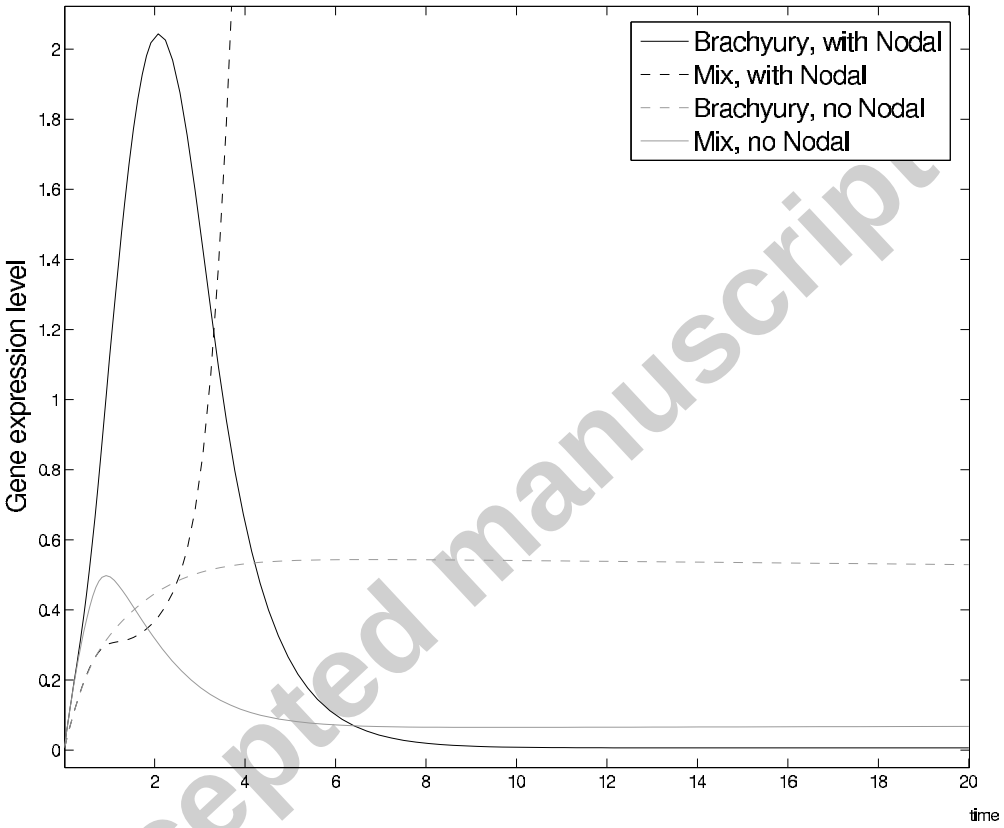

5. Table 1

Protein name(s)	Family Name	Signal/TF	Protein concentration
VegT	-	TF	V
β-Catenin	-	Signal	C
Xnrs 1-6	Nodal	Signal	N
Mixer, Mix.1-2, Bix.1-4	Mix	TF	M
Brachyury	-	TF	B
Goosecoid	-	TF	G
eFGF	-	Signal	E
Siamois	-	TF	S
Lim1	-	TF	L
Activin	-	Signal	A

Variable	Parameter	Value	Variable	Parameter	Value
N	$\lambda_{V,N}$	1	B	$\lambda_{E,B}$	1
	$\lambda_{N,N}$	3		$\lambda_{V,B}$	1
	$\lambda_{C,N}$	1		$\lambda_{X,B}$	10
	$\theta_{N,N}$	1		$\theta_{V,B}$	1
M	$\lambda_{V,M}$	2	G	$\lambda_{LS,G}$	1
	$\lambda_{X,M}$	12		$\lambda_{M,G}$	100
	$\theta_{V,M}$	4		$\theta_{M,G}$	1
	$\theta_{X,M}$	3		$\theta_{G,G}$	1
	$\theta_{B,M}$	1			
S	$\lambda_{C,S}$	1	L	$\lambda_{N,L}$	1
	$\theta_{C,S}$	1		$\theta_{N,L}$	1
E	$\lambda_{B,E}$	12	V	μ_V	.001
	All remaining μ's	1		m	3
	A	5			